NTNU

Norwegian University of
Science and Technology

Hydrotalcite Based Ni-Co Bi-metallic Catalysts for Steam Reforming of Methane

Bilal Yousaf

Chemical Engineering
Submission date: July 2016
Supervisor: De Chen, IKP

Norwegian University of Science and Technology
Department of Chemical Engineering

To My Parents & Family

Acknowledgement

Foremost, I want to express my deepest appreciation to my supervisor, professor De Chen, for his exceptional supervision and valuable research guidance. My profound gratitude goes to him for introducing me to the Catalysis group by offering me the specialization project.

I want to extend my whole-hearted thanks to my co-supervisors, Kumar Ranjan Rout and Shirley Elisabeth Liland for their motivation, encouragement and unparalleled support in every aspect of this project. Specially, Shirley, for her kind support and guidance, whether it was experimental work, result analysis or writing, she helped me at all levels of the project.

I am grateful to Cristian Ledesma Rodriguez and Rauf Salman for their technical support at various stages of this project. I also want to thank John Charles Walmsley, Senior Research Scientist at SINTEF for conducting the TEM analysis of the hydrotalcite catalysts.

I am thankful to my friends and colleagues at NTNU for their support, friendship and a great working environment. I am grateful to be a part of the Katalysis group.

Furthermore, I would also like to acknowledge the role of Catalysis group at the Chemical Department in NTNU for their support in this project for helping me during different phases of the project.

Last but not the least I would like to thank my parents and my family who love me unconditionally and support my every decision. I value their opinion more than anything in my life. This would not have been possible without them.

Abstract

Hydrotalcites or layered-double-hydroxides (LDH) are a class of nanostructured anionic clays. These compounds exhibit high surface areas, high thermal stability and uniform distribution of active metals. Different attempts have been made to study catalysts made from hydrotalcite like precursors for steam reforming.

The study in hand is conducted to evaluate different nickel-cobalt on hydrotalcite catalysts for the steam reforming of methane. A total of four catalysts were synthesized with a fixed nickel to cobalt ratio of 3:7, but with a total metal loading varying from 10-40 wt.%. Preparation was carried out using a co-precipitation method followed by calcination. The final hydrotalcite catalysts were then characterized using XRF, XRD, hydrogen chemisorption, nitrogen adsorption and TPR. The morphology of the catalysts was analyzed by TEM after reduction and passivation. All of the catalysts showed promising results, the formation of hydrotalcite structure was confirmed by XRD profiles. Nitrogen adsorption analysis indicated high surface areas and constant pore size, while hydrogen chemisorption showed constant dispersion and particle sizes.

The kinetic analysis of the samples was conducted in a fixed-bed reactor for the steam reforming of methane. The catalysts were analyzed for mass transfer limitations and an appropriate pellet size was selected for the analysis. It was shown that the methane conversion increased with increased in temperature. Turnover frequency analysis indicated constant activity other than for NiCo-10, while the highest rate of reaction was observed for NiCo-30 and NiCo-40. The selectivity data displayed that the water-gas-shift (WGS) was more pronounced at lower temperature, which was as expected. On the other hand, the reaction order tests indicated that the RDS depends on the methane partial pressure and that there might be a change in the reaction mechanism for NiCo-40, where it is also dependent on the hydrogen partial pressure.

Table of Contents

List of Tables

List of Figures

Abbreviations

BET	Brunauer-Emmett-Teller
BJH	Barrett-Joyner-Halenda
D	Metal dispersion
FEG	Field emission gun
HTS	High temperature shift
FTS	Fischer Tropsch synthesis
GC	Gas chromatography
ICC	International congress on catalysis
ICP-MS	Inductively coupled plasma mass spectrometry
LDH	Layered double hydroxide
LTS	Low temperature shift
RDS	Rate determining step
SMR	Steam methane reforming
Syngas	Synthesis gas
TCD	Thermal conductivity detector
TEM	Transmission electron microscopy
TOF	Turnover frequency
WGS	Water gas shift
XRD	X-ray diffraction
XRD	X-ray fluorescence

Symbols

*	Free site
ΔH^{o}_{298}	Standard heat of reaction at 298 K
θ	Incident angle
λ	Wavelength of the x-rays
A	Pre-exponential factor
A_{CO}	Area under the peak for carbon monoxide
A_{CO2}	Area under the peak for carbon dioxide
A_M	Concentration of the component in the mobile phase
A_S	Concentration of the component in the stationary phase
a_m	Surface area
b	BET constant
C_{CH4}	Methane conversion at specific temperature
c	Speed of light in vacuum
D	Dispersion
d	Distance between diffracting planes
d_{Co}	Particle size of cobalt
d_{Ni}	Particle size of nickel
E	Energy of an accelerated electron
E_a	Activation energy
F_{CH4}	Molar flow of methane
h	Plank's constant
K	Rate constant
K_C	Gas chromatography equilibrium constant
L_{Co}	cobalt metal loading
L_{Ni}	Nickel metal loading
M_{avg}	Average molecular mass
M_{cat}	Mass of the catalyst in the reactor

m	Mass
m_0	Rest mass of an electron
n	Chemisorption stoichiometry
N_A	Avogadro's number
n_A	Amount of reactant
$n_{A,0}$	Amount of reactant at zero time
n_P	Desired product
P	Adsorption pressure
P_0	Saturation pressure at experimental temperature
R	Gas constant
R_x	Rate of reaction at a specific temperature
R_{CO}	Response factor for carbon monoxide
R_{CO2}	Response factor for carbon dioxide
S_{CO}	Carbon monoxide selectivity
S_P	Product selectivity
T	Temperature in Kelvins
V_a	Adsorbed volume
ν_A	Stoichiometric coefficient of reactant
ν_P	Stoichiometric coefficient of product
v_m	Molar volume
x	Angle of reflection (integer)

1 Introduction

The modern evolution of technology and the rapid development of industry have most demanding energy requirements. Data analysis from British petroleum's 'Statistical review of world Energy' shows that, world energy consumption is increasing linearly since last many decades, **Figure 1.1**. There is an increasing need for the development of new methods and technologies to fulfill the energy demands. New sources of energy are not only required to be able to satisfy the energy demands but should also be environmental friendly.

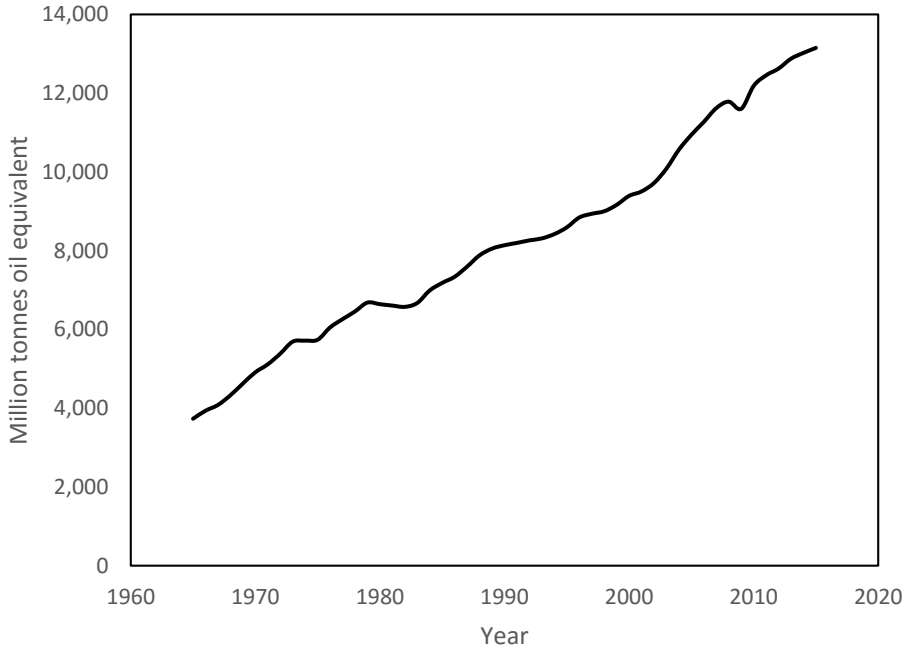

Figure 1.1: World primary energy consumption data. British petroleum, Statistical Review of World Energy (1965-2015) [1]

Hydrogen has been identified as one of the major prospective candidates to carry out the world energy demands. Although, hydrogen is one of the most abundant elements in nature yet its scarce in its free form. This makes it an energy carrier instead of a direct source of energy [2]. Most of the carried out research is focused on developing a cost effective and efficient process for the production of hydrogen.

Hydrogen is present all around, earth's water mass contains 11.2 wt. %, other organic matter like fossils i.e. natural gas, oil and coal also contain hydrogen. Natural gas is one of the major sources of hydrogen, it carries from traces up to 40 vol. % [2]. Hydrocarbons from natural gas are used to produce hydrogen on an industrial scale. Water is also an important source of

hydrogen. Using an external energy source hydrogen can be produced either from hydrocarbons or water or a mixture of both of these. Methane from natural gas reacts with water in an endothermic reaction producing carbon monoxide and hydrogen.

Today, industrially hydrogen is being produced from a variety of different processes. Steam reforming is one of the major processes for the production of hydrogen. Other methods include electrolysis of water, gasification of coal and partial oxidation of oil. Only in 2006, 11 million tons of hydrogen was produced by the USA alone [3]. It is also estimated that the commercial market for hydrogen is now 100 billion dollars [4].

Steam reforming is an endothermic reaction of steam and hydrocarbons (methane) to give a mixture of hydrogen, carbon monoxide, carbon dioxide and unconverted methane and steam. The reforming reactions are also accompanied by the water gas shift reaction [5]. The mixture of hydrogen, carbon monoxide, carbon dioxide is known as syngas, and has great industrial significance. It is used in the production of chemicals like ammonia and methanol. It is utilized by Fischer-Tropsch Synthesis to convert to fuels and by water-gas-shift reaction it can be used to recover hydrogen.

Different catalysts are used to enhance the steam reforming process. Materials like platinum, palladium, ruthenium and rhodium can be used as catalysts. But, Nickel based catalysts are found to be the most economically feasible for the process [6]. Iron and cobalt catalysts have more activity but are easily oxidized under process conditions. Typically, a nickel based catalyst on alumina or magnesium oxide support is used [6].

Hydrotalcites or aluminum-magnesium layered double hydroxides is a family of synthetic compounds. It contains double layers similar to magnesium hydroxide $Mg(OH)_2$-, where divalent cations have been replaced by trivalent cations. This leads to positively charged sheets stacked together, which are kept neutral by the inserted anions. Although, hydrotalcites have different varieties yet only aluminum-magnesium hydrotalcites have been studied majorly as a catalyst support [7].

1.1 Background

This study is a continuation of a previous project [8], where a set of hydrotalcite catalysts was prepared by varying the nickel to cobalt ratio and keeping the overall metal loading constant at 12 wt.%. Based on the results, it was concluded that the nickel-cobalt hydrotalcite catalysts had higher activity as compared to pure nickel or cobalt hydrotalcite catalysts. Also, the optimum nickel to cobalt ratio was selected to be 3:7. The results of the reference study are presented as

a poster at ICC, Beijing in July, 2016. The reference will be made throughout this report to the poster and wherever needed the actual results will be presented either in text or in appendices. The set of catalysts prepared for this study are based on that optimal nickel to cobalt ratio, varying the overall metal loading.

1.2 Scope of the study

Nickel-cobalt based hydrotalcites, pure or promoted to enhance certain properties have been studied for processes like sorbent enhanced steam reforming (SESR) and steam reforming of Ethanol, Biomass and other compounds [7] [9] [10]. These catalysts have the following advantages as compared to other catalysts,

- Complex oxides prepared from hydrotalcites have been known to exhibit large metal surface areas, high thermal stability and uniform distributions of the active species [11] [12] [13] [14] [15].
- Catalyst prepared from Ni/Al hydrotalcite-like compounds exhibit higher catalytic stability due to higher nickel dispersion, smaller nickel particle size and the stronger metal-support interaction leading to stronger resistance to coke deposition [12].

The objective of the project is to study hydrotalcite based bi-metallic catalysts for the steam reforming of methane. The purpose is to screen a best catalyst based on the characterization results and the kinetic analysis. The hydrotalcite catalysts are synthesized and then the different catalytic properties are analyzed using various characterization techniques. The kinetic study of the hydrotalcite catalysts is also carried out to test the catalysts in the steam reforming set-up.

2 Theory

2.1 Steam reforming of methane (SMR)

Steam reforming is a chemical process in which a hydrocarbon rich feedstock is converted to hydrogen and syngas (hydrogen, carbon monoxide and carbon dioxide) [6]. Syngas is an important industrial raw material, it is used to produce a wide variety of commercially significant products like methanol and other higher alcohols and some synthetic fuels in Fischer-Tropsch synthesis. The success of the steam reforming process lies in the cheap and rather extensive availability of methane all over the world [6]. Steam reforming was developed in the beginning of the 20th century in Germany to produce hydrogen for ammonia synthesis. Further developments were made when natural gas, naphtha and other feedstocks were introduced later in 1930s [6].

Although steam reforming is used to convert fuels like methanol, ethanol and biomass etc., but for the purpose of this study only steam reforming of methane will be discussed here.

2.1.1 Steam reforming process

The steam reforming of methane is an endothermic process in which high temperatures up to 1000 °C and moderate pressures 25-30 bar are implied [6]. Although the process is carried out at high temperatures yet a catalyst is needed due to high stability of methane [16]. The process is carried out in a tubular reactor in a vertical position. The heat required by the reaction is supplied by a furnace which surrounds the reactor [6].

In a relatively new technique, some of the methane is burned at the entrance of the reactor. This supplies the heat required to carry out the reaction, this is called auto-thermal reforming [6].

2.1.2 Water-Gas-Shift (WGS) Reaction

An important feature of the hydrogen production through steam reforming is the water-gas-shift reaction. The reaction is given in Equation (2.1), where carbon monoxide reduces steam to hydrogen and is oxidized to carbon dioxide [17],

$$CO + H_2O \leftrightarrows CO_2 + H_2;\ \Delta H^{\circ}_{298} = -41\ kJmol^{-1} \tag{2.1}$$

Being opposite to the steam reforming, the WGS reaction is favored at lower temperatures owing to its moderate exothermic nature. However, at low temperatures, the reaction is kinetically limited, the equilibrium constant decreases as temperature increases. Industrially, to overcome this limitation and to maintain high reaction rates, the reaction is carried out in

two stages to achieve high conversion. High temperature shift (HTS) reaction in the first step takes place between 300 to 500 °C, using an iron oxide/chromia catalyst. In this step the carbon monoxide outlet concentration is reduced to 3 vol. %. Second step converts the remaining carbon monoxide in a low temperature shift (LTS) at 210 to 250 °C, over a high activity $Cu/ZnO/Al_2O_3$ catalyst [17].

2.1.3 Coke formation

One of the main challenges related to steam reforming, is the coke formation. Several reactions can cause coke formation, which deposits on the catalyst. For economic reasons, lower steam content is favorable which leads to decreased oxidation potential thus increasing the probability of carbon formation [6]. Coke formation is necessary to suppress using appropriate conditions because of the fact that carbon deposits on catalysts thus blocking the active sites, leading to deactivation. Also, coke formation blocks reformer tubes thus giving rise to hot spots [16].

Coke formation is suppressed by implying excess steam, usually the process is carried out at steam to carbon ratio of 2.5 to 4.5 moles of H_2O per moles of carbon. Whereas, the upper limit applies to higher hydrocarbons. Since the addition of excess steam also lowers the partial pressure of hydrocarbons in the reaction thus increasing their conversion [16].

2.1.4 Methane slip

Because of the requirement of syngas to be at high pressure most of the steam reformers are operated at high pressure. Although this makes the economically favorable yet it is thermodynamically unfavorable. The advantages are lower cost of syngas compression and compact reformer size, achieved at the cost of methane conversion. This is countered by using high temperatures and excess steam. The effect of pressure and excess steam on methane slip is shown in **Figure 2.1** [16].

A constraint is placed on the temperatures and pressures that can be implied. The maximum operating temperatures at a given pressure are limited, based on the creep limit of reformer tubes. Still, an appreciable amount of methane can be found at typical reforming temperatures and pressures. A lower methane slip is favorable for the economics of the process. The high temperatures favored for the process could be accommodated by using high strength materials for reforming tubing [16].

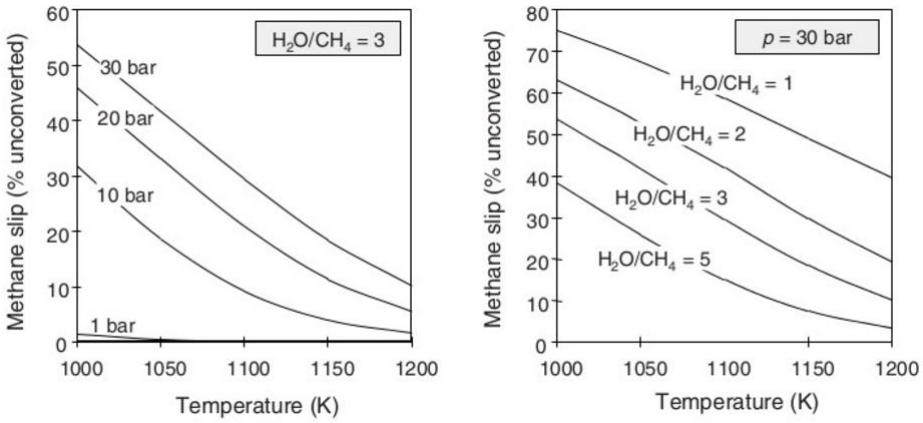

Figure 2.1: Effect of pressure (left) and steam to methane feed ratio (right) on methane slip as a function of temperature [16]

2.1.5 Reactions and Thermodynamics

Steam reforming of methane according to Equation (2.2), while Equation (2.3) is a general reaction for all steam reforming of all hydrocarbons [6],

$$CH_4 + H_2O \leftrightarrows CO + 3H_2;\ \Delta H^{\circ}_{298} = +206\ kJmol^{-1} \tag{2.2}$$

$$C_nH_m + nH_2O \leftrightarrows nCO + \left(n + \frac{m}{2}\right)H_2;\ \Delta H^{\circ}_{298} > 0\ kJmol^{-1} \tag{2.3}$$

Other side reactions are [16],

$$CO + H_2O \leftrightarrows CO_2 + H_2;\ \Delta H^{\circ}_{298} = -41\ kJmol^{-1} \tag{2.4}$$

$$CH_4 + CO_2 \leftrightarrows 2CO + H_2;\ \Delta H^{\circ}_{298} = +247\ kJmol^{-1} \tag{2.5}$$

$$CH_4 \leftrightarrows C + 2H_2;\ \Delta H^{\circ}_{298} = +75\ kJmol^{-1} \tag{2.6}$$

$$2CO \leftrightarrows C + CO_2;\ \Delta H^{\circ}_{298} = -173\ kJmol^{-1} \tag{2.7}$$

Steam reforming of methane is highly endothermic and hence requires energy in the form of heat. The main reaction can be accompanied by coke formation. This coke formation could either be due to the decomposition of methane Equation (2.6) or disproportionation of carbon monoxide Equation (2.7). Coke formation is the main challenge related to steam reforming of methane leading to deactivation of the catalyst [16].

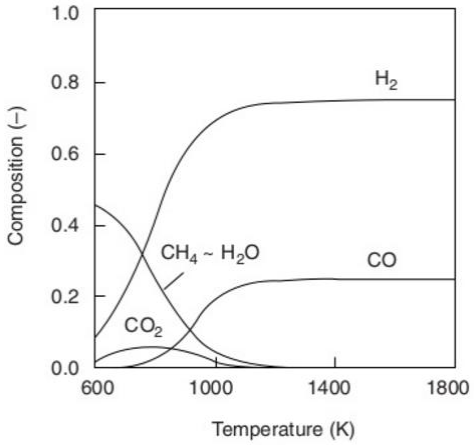

Figure 2.2: Equilibrium gas composition at 1 bar as a function of temperature: Steam reforming of Methane, H_2O/CH_4=1 mol/mol, H_2O curve coincides with CH_4 curve [16]

In **Figure 2.2**, equilibrium compositions for steam reforming of methane are shown at 1 bar as a function of temperature, here stoichiometric amounts of steam and methane are used. At equilibrium, hydrogen and carbon monoxide increase with increasing temperature, due to the endothermic property of reactions (2.2) and (2.5). Also, carbon dioxide goes through a maximum with increasing temperature. Because, it is produced in the exothermic WGS reaction (2.4), and partly consumed in the dry reforming reactions (2.5) [16].

2.1.6 Steam reforming mechanism

Methane has a symmetrical and highly stable structure. The activation of the methane is carried out in a direct dissociative adsorption step, Equation (2.8). This is associated with substantial energy and entropy barriers. It been shown in some studies that the rate determining step varies between the dissociative adsorption and Equation (2.14) [6]. The overall reaction scheme is [6],

$$CH_4 + 2 * \longrightarrow CH_3^* + H^* \quad (2.8)$$

$$CH_3^* + * \leftrightarrows CH_2^* + H^* \quad (2.9)$$

$$CH_2^* + * \leftrightarrows CH^* + H^* \quad (2.10)$$

$$CH^* + * \leftrightarrows C^* + H^* \quad (2.11)$$

$$H_2O + 2 * \leftrightarrows HO^* + H^* \quad (2.12)$$

$$HO^* + * \rightleftarrows O^* + H^* \quad (2.13)$$

$$C^* + O^* \leftrightarrows CO^* + *$$ (2.14)

$$CO^* \rightleftarrows CO + *$$ (2.15)

$$2H^* \rightleftarrows H_2 + 2*$$ (2.16)

A free site is indicated by a (*).

2.2 Catalysts for steam reforming of methane

Being a highly endothermic process, steam reforming is carried out at high temperatures. Although a catalyst is still required, pertaining to the high stability of the methane molecule [16]. The metals from group VIII are active choices for the steam reforming of methane. Nickel in addition to iron and cobalt is preferred. Cobalt oxidizes easily under normal steam reforming conditions and iron requires a strong reducing environment. Rhodium and ruthenium have more activity as compared to nickel, while other noble metal have activities in between [5].

Alkalis' suppress the activities of group VIII metals. Since, presence of an alkali increases the adsorption of carbon monoxide thus resulting in poisoning of the catalyst. Industrial catalysts are exposed to extreme conditions of temperature and pressure like 30 bars and 600 °C. The support should be able to withstand such conditions without losing strength [5].

2.2.1 Nickel catalysts

Nickel is the widely preferred catalyst for steam reforming of methane. Nickel and some other noble metal catalysts supported on metal oxides have been discovered to have high activity and selectivity for hydrogen production. Nickel is prioritized based on its high activity for C-C and O-H bond breaking and its facilitation to form molecular hydrogen; hydrogenation. Coke formation, as discussed in section **2.1.3**, is a major concern for SMR. The rate of carbon deposition was found to be retarded when nickel promoted catalysts were used for steam reforming of methane [18].

Coke formation and sintering of metal particles deactivated the industrial nickel catalysts. Metal surface area and catalytic activity is reduced due to sintering, this also promotes coke formation. Coke formation can be reduced by modifying the catalyst support. It was found that acidic support had more coke formation as compared to basic or basic species containing support [18].

2.2.2 Cobalt catalysts

Cobalt catalysts have properties comparable to noble metals for SMR and WGS reactions. Commercial cobalt catalysts can be deactivated by the impurities like sulfur and chlorine compounds. This makes them ineffective for WGS reaction of coal based syngas [17].

There are 3 phases of cobalt; Co^{+3}, Co^{+2} and Co^{0}. In case of cobalt supported on magnesium oxide only metallic cobalt was found to be available for SMR. When compared to nickel and rhodium, cobalt had higher activity and selectivity for hydrogen formation at lower temperatures [18].

Effect of support was studied on 12 % cobalt supported on titanium oxide, silicon oxide and alumina. These supports had great effects on the activity and selectivity at lower temperatures. Another study showed that, greater stability was attributed to the removal of carbonaceous deposits [18]. It was also found out that nickel supported on magnesia had superior activity and selectivity for hydrogen as compared to cobalt catalysts for steam reforming of methane [17].

2.2.3 Bimetallic catalysts

Bimetallic catalysts are usually inorganic oxide supported bimetallic nanoparticles. These are used as catalysts in various processes due to the positive effects of metal interactions. Some of the processes that have been studied using bimetallic catalysts are, Fischer-Tropsch synthesis, selective hydrogenations and hydrogen production reactions [19].

The interactions between main component metal M_1 and added component metal M_2 give rise to surface effects these surface effects are divided into geometric and electronic effects. these effects have important effect on the catalytic activity, since most reactions are dependent on the surface atoms [19]. The electronic effect which is due to the difference in electronic affinity of the metals. This electronic effect may affect the adsorption and desorption of reactants, products and intermediates which can highly influence activity and selectivity of reactions [19].

Bimetallic catalysts can increase the resistance to coking by decreasing the C solubility of the nanoparticles or by increasing the C gasification activity [19]. This reduced coking effect is also observed in hydrotalcites [17].

2.2.4 Hydrotalcite

Hydrotalcite is a naturally occurring anionic clay mineral, it is the hydroxyl-carbonate of magnesium and aluminum. Hydrotalcites have exchangeable anions and are also called layered double hydroxides (LDH). The structure is similar to ($Mg(OH)_2$)- like layers in which some of

the divalent cations have been replaced with trivalent ones. Due to this phenomena, hydrotalcite contains positively charged sheets stacked together. These positively charged sheets are kept neutral by the inserted anions between them, as shown in **Figure 2.3** [7]. The ion exchange capabilities of hydrotalcites are due to the charge balancing anions that lie between structural layers. Hydrotalcites have the general formula [17],

$$\left[M_n^{+2}M_m^{+3}(OH)_{2(m+n)}\right]^{+m}\left(A_{m/x}^{x}\right) * yH_2O \qquad (2.17)$$

When exposed to high temperatures, hydrotalcites are converted into small crystal sized mixture of interactive metal oxides. These metal oxides have specific properties like high specific surface area, high dispersion, well dispersed active sites and high thermal stability [17]. Hydrotalcite catalysts exhibit a memory-effect when calcination temperature is below a certain temperature the hydrotalcite structure is retained when exposed to water. However, if the temperature is sufficient then the oxide structure is permanent.

Hydrotalcites have been used as wide range catalysts for reactions such as water-gas-shift reaction, steam reforming of methane, alkylation and bio-diesel conversion. When used for SMR, hydrotalcites are more resistant to coke formation and sintering as compared to catalysts supported on alumina. Nickel supported on hydrotalcite catalysts have been studied to be more stable at severe conditions [17].

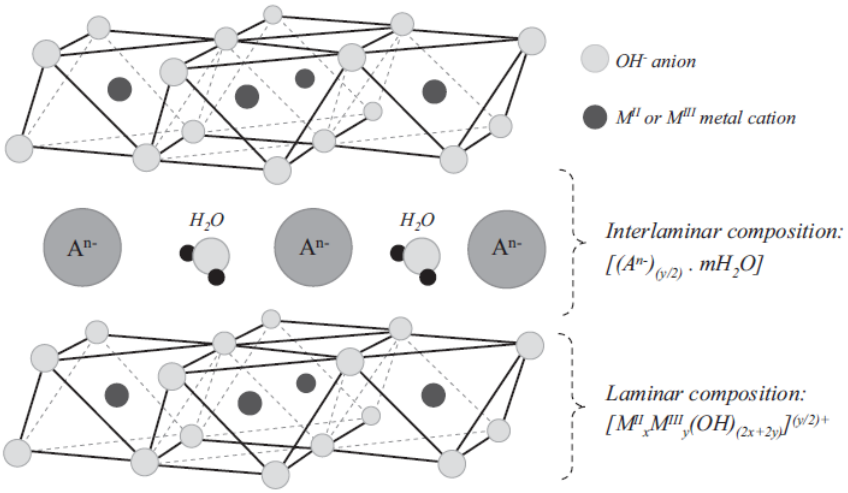

Figure 2.3: Schematic representation of hydrotalcite structure [7]

CoO/NiO/MgO/Al_2O_3 present in nickel-cobalt hydrotalcite after calcination is found to be converted to Co/Ni/MgO/Al_2O_3 when reduced. The composition of the hydrotalcite was determined by its reduced form.

2.3 Catalyst synthesis

2.3.1 Co-precipitation

Co-precipitation is a synthesis method in which a solute is precipitated out of a solution under the effect of an added carrier. The added carrier makes the solute bind together instead of staying dispersed. In case of more than one metallic compounds, the composition of the precipitate depends on the difference in solubility of the components and the chemistry of precipitation [20].

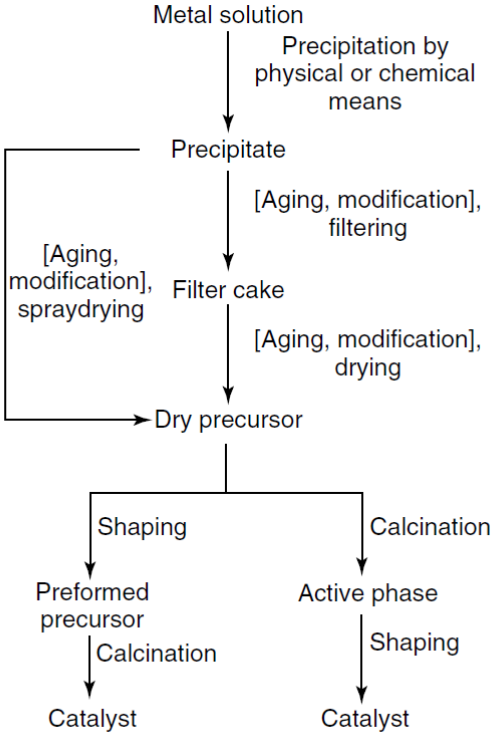

Figure 2.4: Preparation scheme for precipitated catalysts. Optional steps are indicated by square brackets [5]

Co-precipitation is a suitable technique to synthesize homogenously distributed catalyst components, it can also be used for the preparation of precursors with definite stoichiometry, which can be easily converted to catalyst. Well mixed crystallites of the components can be obtained by calcination or reduction. Such dispersion of catalyst components is hard to achieve with other types of precipitations, which makes co-precipitation an important technique in solid catalyst synthesis [5].

When implying co-precipitation, sufficient knowledge of relative solubilities of the precipitates, and the possibility of the formation of defined mixed phases is important. In the case of wide difference in solubilities of the components, sequential precipitation might occur

and leading to concentration gradients in the product. To avoid this problem, precipitation is carried out at high super saturation. The resultant is a defined, insoluble product, like Hydrotalcite as in the case of Nickel and Aluminum [5].

2.3.2 Calcination

Calcination is a thermos-chemical treatment step in the formation of catalysts. During calcination, catalysts are heated in the presence of oxygen under well-defined conditions. This treatment converts the precursors into the final catalyst by formation of a strong chemically bonded network. Calcination induces the solid state reactions necessary for the final stability of the material [5].

2.3.3 Reduction

Reduction is a chemical procedure implied to selectively remove oxygen from a chemical component. In catalysis reduction is used to impart specific properties to the catalyst. Reduction leads to a highly porous material, in the reduced catalyst loading with the active component is no less than 96-98 wt. % while the mechanical strength is extremely high [5].

2.4 Catalyst characterization

Below is a theoretical background of the characterization techniques used for the analysis of hydrotalcite catalysts.

2.4.1 X-Ray Fluorescence (XRF)

X-ray fluorescence is a technique used for the qualitative and quantitative analysis of materials. The XRF analysis is a simple and fast analysis, which is applicable to a wide range of components. XRF is a recognized technique used for the determination of accurate analysis of a material. The concentration of an element is the combination of calibration constant, measured peak intensity and correction term. The effects of absorption and enhancement are accounted in the correction term [21].

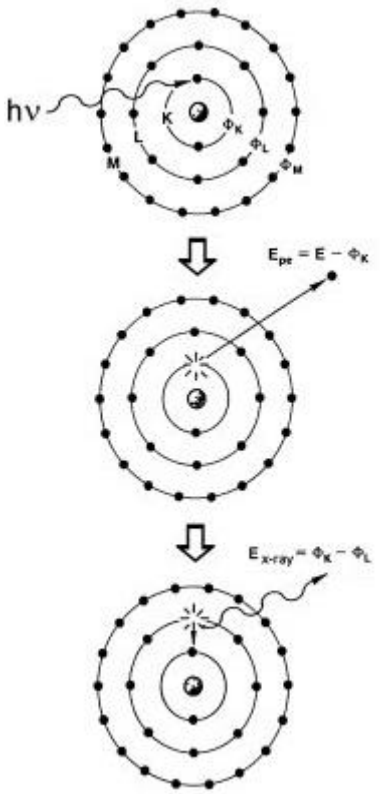

Figure 2.5: The XRF Process [22]

If a photon (*hv*) with sufficient energy strikes an electron it can expel the electron from its orbital. This is only possible when the photon has striking energy more than the binding energy of the electron to its nucleus. When an electron is expelled from an inner orbital, an electron from a higher orbit will come to take its place by emitting a photon. The energy of the emitted photon will be equal to the energy difference of the two orbitals and will be the characteristic x-ray of the element. The element can be identified when the energy of its characteristic x-ray is known [22].

For a particular energy (wavelength) of emitted x-ray, number of emitted photons per unit time (peak intensity) is related to the amount of the particular element in the sample. The number of emitted photons for a particular time are calculated by counting, and displayed as semi-Gaussian peaks [22].

2.4.2 Temperature programmed reduction (TPR)

Temperature programmed reduction, TPR, is a technique widely used, to find out the efficient reduction conditions. Calcination is carried out for thermal decomposition. In case of improper calcination, sintering may occur. The process is performed under controlled heating in

hydrogen flow because of the ease of the removal of the reduction product i.e. water. Following is the chemical reaction equation is for metals undergoing reduction [29],

$$MO_n + H_2 \longrightarrow M + nH_2O \tag{2.18}$$

The results of TPR are usually discussed in a qualitative manner due to the process being quite complex [5]. The information obtain from the TPR analysis is the temperature required for the complete reduction of the sample, either the reduction is single or multiple step and the effects of promoters and support.

2.4.3 Hydrogen Chemisorption

Chemisorption in a process in which adsorbate forms chemical bonds with the adsorbent. Catalysts are highly porous materials having high specific surface area. The surface of the catalysts may contain finely divided metal particles. The dispersion of these metal particles on the surface of catalysts can be analyzed using chemisorption [23].

For chemisorption, titration method is used; a reactive gas like hydrogen or carbon monoxide is along with a carrier gas like helium in the form of pulses [23]. Hydrogen, adsorbs on most materials in a dissociative manner [5],

$$H_2 + 2M \rightarrow 2M - H \tag{2.19}$$

The pre-treated catalyst is evacuated and contacted with a known quantity of the reactive gas [5]. The reactive gas is injected into the reactor in the form of pulses repeatedly, these pulses get chemisorbed on the catalyst. The quantity of reactive gas chemisorbed decreases for each succeeding pulse. The composition at the outlet of the reactor is measured using thermal conductivity detectors. Cumulative quantity is the sum of all the proportions of all the pulses.

The quantity of a gas adsorbed selectively on the catalyst surface gives the surface area and metal dispersion, depending if the stoichiometry is known [5]. Adsorption isotherms are obtained by increasing pressure and determining the quantity of the reactive gas adsorbed. The quantity adsorbed at mono-layer coverage can be found by extrapolating the isotherm to zero pressure. The surface area and metal dispersion is given by the following equations [5],

$$A = \frac{v_m}{22414} N_A \frac{n}{m} a_m \frac{100}{wt} \tag{2.20}$$

$$D = \frac{\frac{v_m n}{22414m}}{\frac{wt}{100M}} \tag{2.21}$$

Where, v_m is expressed in cm^3 (STP), N_A is the Avogadro's number, n the chemisorption stoichiometry, m the mass of the sample (g), a_m the surface area (m^2) occupied by a metal atom and wt (%) the metal loading [5].

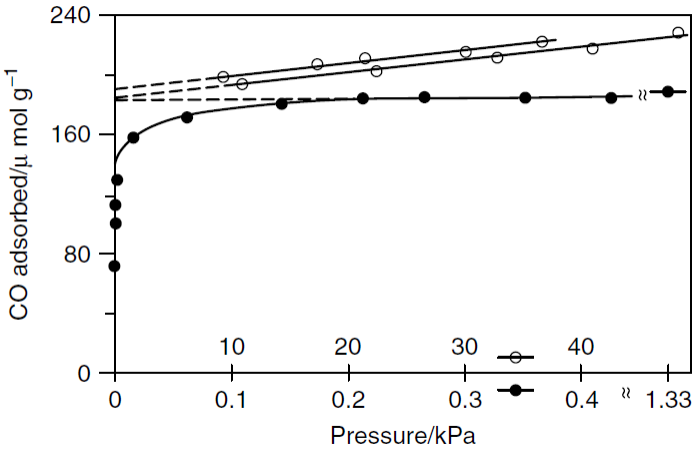

Figure 2.6: Isotherms for the adsorption of CO on EUROPT-1 Pt/SiO_2 catalyst at room temperature from different laboratories for a pressure range 0 – 1.33 kPa (solid circles) and 10 – 50 kPa (open circles) [5]

Using the value of D and assuming spherical particles, the particle size d_{Co} and d_{Ni} was calculated as follow [18],

$$d_{Co} = {}^{96}/_{D}\ [nm] \tag{2.22}$$

$$d_{Ni} = {}^{101}/_{D}\ [nm] \tag{2.23}$$

For a mixture of nickel and cobalt, the average particle size is given by [18],

$$d_{Co-Ni} = \left[{}^{96}/_{D}\right] x \left[{}^{\%Co}/_{100}\right] + \left[{}^{101}/_{D}\right] x \left[{}^{\%Ni}/_{100}\right]\ [nm] \tag{2.24}$$

2.4.4 Nitrogen Adsorption

Brunauer Emmett Teller (BET) theory is used for the measurement of internal/specific surface area of a material. BET refers to multi-layered adsorption as an extension to Langmuir's isotherm [24], in which gives the quantity of adsorbed gas varies with equilibrium pressure at constant temperature. The internal surface area can be calculated by using the total number of adsorbed gas molecules and the surface area occupied by each molecule.

For BET surface area calculation [25],

1. Adsorption isotherm is converted to BET plot and BET mono-layer capacity is calculated.
2. Specific surface area is calculated based on the molecular area.

The assumptions for BET theory are the same as Langmuir's isotherm;

- The gas molecules adsorb on a solid surface in the form of layers
- There is no interaction between layers, and
- The Langmuir's theory holds for each layer

Based on these assumptions the BET equation is [24],

$$\frac{P}{V_a(P_0 - P)} = \frac{1}{bV_a} + \frac{(b-1)}{bV_a}\frac{P}{P_0} \tag{2.25}$$

Where, P is the adsorption pressure, P_0 is the saturation pressure at experimental temperature, V_a is the total volume adsorbed at P and b is the BET constant.

For the BET surface are calculation, first the adsorption isotherm is converted to BET plot. In a BET plot, Equation (2.25) is plotted as a straight line with (P/P_0) on the x-axis and [$P/V_a(P_0$-P)] on the y-axis. This is then used to calculate the BET monolayer capacity. Then the specific surface area is calculated using molecular area. By knowing the area occupied by a single molecule, the number of molecules adsorbed are calculated from the monolayer coverage. Which can then be used to calculate the specific surface area [5].

Barrett, Joyner, and Halenda gave a method for the determination of pore size distribution. The method involves using experimental isotherms and implying modified Kelvin equation. The amount of adsorbate removed from the pores when the relative pressure is decreased is related to the size of pores. The method applies only to the meso-pore and macro-pore size range [26] [27].

2.4.5 X-Ray Diffraction (XRD)

X-Ray Diffraction (XRD) is one of the most important techniques widely used for catalyst characterization. XRD is used for the identification of crystalline structure, and for particle size estimation. Depending on the different planes and angles within every structure, different components in the sample have their own unique diffraction patterns. These patterns are used to identify the structure of the sample.

The constructive interference of the x-ray waves and secondary spherical waves spread from the scattering source, in different directions is given by Bragg's Law [28],

$$2dsin\theta = x\lambda \tag{2.26}$$

Where, d is the distance between diffracting planes, θ is the incident angle, x is an integer (angle of reflection) and λ is the wavelength of the x-rays.

2.4.6 Transmission electron microscopy (TEM)

Transmission electron microscopy refers to transmitting a beam of electrons though an ultra-thin specimen. When this beam interacts with the specimen the resulting image is magnified and focused on an imaging device. Significantly higher resolution is possible by the use of TEMs as compared to light microscopes [30].

Theoretically, the maximum resolution achievable by a light microscope is limited by the wavelength of the photons. TEM overcame this limitation by using electrons. Since electrons behave as waves and particles 'Louis Victor de Broglie hypothesis'. The de Broglie equation relates the wavelength of the electrons to their kinetic energy as [30] [31],

$$\lambda_e = \frac{h}{\sqrt{2m_0E\left(1+\frac{E}{2m_0c^2}\right)}} \tag{2.27}$$

Where, h is the Plank's constant, m_0 is the rest mass of an electron, E is energy of an accelerated electron and c is the speed of light in vacuum. Electron microscopes use thermionic emission to generate electrons from a filament, usually Tungsten [30].

2.5 Activity and selectivity measurement

2.5.1 Rate of reaction

The rate of reaction is a very wide topic in the field of chemistry. It defines the speed of a chemical reaction. The speed of the chemical reaction is usually defined as the rate of disappearance of reactants or the rate of formation of products [6]. The reaction rate was calculated using Equation (2.28),

$$R_x = \frac{C_{CH_4}xF_{CH_4}}{M_{cat}} \tag{2.28}$$

Where, R_x is the rate of reaction, C_{CH4} is the methane conversion at that temperature, F_{CH4} is the molar flow of methane at that temperature and M_{cat} is the mass of the catalyst in the reactor.

2.5.2 Selectivity

The selectivity is the amount of reactant converted to the desired product. It is expressed as a ratio of the quantity of the desired product to the quantity of the reactant converted. The information about the course of reaction is obtained from selectivity, since parallel or sequential side reactions might be occurring at the same time. Equation (2.29) is the general formula to calculate selectivity [32],

$$S_P = \frac{n_P|v_A|}{(n_{A,0} - n_A)v_P} \tag{2.29}$$

Where, S_P is the product selectivity, n_P is the desired product, $n_{A,0}$ is the amount of reactant at zero time, n_A is the current amount of reactant and v_A and v_P are the respective stoichiometric coefficients of the reactant and desired product. For the purpose of this study the carbon monoxide selectivity was calculated from Equation (2.30),

$$S_{CO} = \left[\frac{A_{CO}xR_{CO}}{A_{CO}xR_{CO} + A_{CO_2}xR_{CO_2}}\right]x100 \tag{2.30}$$

Where, S_{CO} is the carbon monoxide selectivity, A_{CO} is the area under the peak for carbon monoxide, R_{CO} is the response factor for carbon monoxide, A_{CO2} is the area under the peak for carbon dioxide and R_{CO2} is the response factor for carbon dioxide. Only the carbon monoxide selectivity was examined, since selectivity of carbon dioxide directly depends on the selectivity of carbon monoxide, as,

$$S_{CO_2} = 1 - S_{CO} \tag{2.31}$$

Selectivity has significant importance in the industrial catalysis. As in the case of syngas, different products are obtained for different catalysts used [32].

2.5.3 Turnover frequency (TOF)

The activity of a catalyst is measured by number of molecules converted per active site per unit time called Turnover frequency (TOF). TOFs values of commonly implied catalysts are usually one per cycle. The lifetime of a catalyst is defined, as the number of turnovers before the catalyst cease operating [5]. For heterogeneous catalysts the number of active centers is derived usually from sorption methods Equation (2.32) [32],

$$TOF = \frac{Volumetric\ rate\ of\ reaction}{number\ of\ centers/_{volume}} = \frac{moles}{volume.time}\frac{volume}{moles} = time^{-1} \quad (2.32)$$

For this study, the turnover frequency at a specific temperature was calculated using Equation (2.33),

$$TOF = \frac{RxM_{avg}}{(L_{Ni} + L_{Co})xD} \quad (2.33)$$

Where, R is the rate of reaction at that temperature, M_{avg} is the average molecular weight, L_{Ni} is the nickel metal loading, L_{Co} is the cobalt metal loading and D is the dispersion.

2.5.4 Arrhenius equation

Arrhenius equation can be physically interpreted, in case of a reaction when potential energy barrier exists and has to be crossed for the reaction to occur. For an elementary reaction, the temperature dependence of the rate constant is shown by using the Arrhenius equation [6], the relation is shown in Equation (2.34),

$$K = Ae^{-E_a/_{RT}} \quad (2.34)$$

Where, K is the rate constant, A is the pre-exponential factor, Ea is the activation energy, R is the gas constant and T is the temperature in Kelvins. The temperature dependence is only in the exponential term of the equation and that the pre-exponential factor is a constant [6].

The activation energy can be determined from the data obtained by plotting the natural log of the rate constant versus inverse of the temperature. Hence, taking natural log of Equation (2.34) and rearranging gives,

$$\ln(K) = \ln(A) + \left(\frac{-E_a}{R}\right)T \quad (2.35)$$

Equation (2.35) refers to the equation of straight line, here the calculated TOF values can be plotted in Arrhenius coordinates, i.e. ln(TOF) versus 1/ T. The slope of this plot will yield activation energy and the incept will give the pre-exponential factor.

2.5.5 Gas chromatography

Gas chromatography is an analytical technique in which two phases are implied; first is a stationary bed with a large surface area and second is a gas, which moves across the bed. The mobile phase is usually an inert gas like helium and the stationary phase is a high boiling liquid coated on the insides of a capillary column. The vaporized sample is carried by the gas through

the stationary bed. The components of the sample separate out onto the stationary bed on the basis of their respective solubilities at a given temperature [33].

The components more soluble in the mobile phase as compared to the stationary phase tend to appear on the outlet faster as compared to the components with less solubility in the gas phase. Eventually the components leave the system and enter a detector. The output signal of the detector gives rise to a chromatogram. The equilibrium constant K_C expresses the tendency of a component to be attracted to the stationary phase. Given as [33],

$$K_C = \frac{A_S}{A_M} \tag{2.36}$$

Where, K_C is the equilibrium constant, A_S is the concentration of the component in the stationary phase and A_M is the concentration of the component in the mobile phase. The equilibrium constant is directly proportional to the solubility of the component in the stationary phase.

An important term that is used for the measurement of outlet gas concentration is the response factor, it is defined as the ratio between the concentration of a compound being analyzed and the response of the detector to that compound. The chromatogram shows response from the detector as a peak, although there are several ways to quantify a peak, one of the most common is the peak area [34]. Thus,

$$Response\ factor = {Peak\ area}/{Concentration} \tag{2.37}$$

3 Experimental

In this section the experimental procedures that were followed for the synthesis, characterization and the kinetic analysis of the catalysts are described in detail.

3.1 Materials

The materials used for the synthesis of nickel cobalt hydrotalcites are given below in **Table 3.1**.

Table 3.1: Details of the reactant materials

Materials	Chemical Formulae	Mol. Weight	Purity [%]	Manufacturer
Nickle nitrate hexahydrate	$Ni(NO_3)_2.6H_2O$	290.79	99	Sigma Aldrich
Cobalt nitrate hexahydrate	$Co(NO_3)_2.6H_2O$	291.03	>98	Acros Organics
Magnesium nitrate hexahydrate	$Mg(NO_3)_2.6H_2O$	256.41	99	Sigma Aldrich
Aluminum nitrate nonahydrate	$Al(NO_3)_3.9H_2O$	375.13	>=98	Sigma Aldrich
Sodium hydroxide	NaOH	39.99	>98	Merck
Sodium carbonate	Na_2CO_3	105.98	100	VWR Chemicals

3.2 Catalyst synthesis

For the purpose of this study, catalysts were synthesized using the co-precipitation technique. In total four catalysts were prepared keeping the nickel to cobalt ratio constant at 3:7 and varying the overall metal loading from 10 to 40 wt.%. The details of the catalysts prepared are presented in **Table 3.2**. The detailed calculations and amount of the reactants is given in **Appendix A**.

Table 3.2: Percentage of Ni and Co in prepared catalysts

Catalyst	Total metal loading [wt.%]	Nickel [wt.%]	Cobalt [wt.%]
NiCo-10	10	3	7
NiCo-20	20	6	14
NiCo-30	30	9	21
NiCo-40	40	12	28

3.2.1 Co-precipitation

An anion solution was prepared using aluminum nitrate nonahydrate, magnesium nitrate hexahydrate, cobalt nitrate hexahydrate and nickel nitrate hexahydrate in a 3-necked flask. The cation solution was prepared using sodium carbonate and sodium hydroxide. Both solutions were prepared in 400ml de-ionized water. The cation solution was then pumped into the anion solution for 2 hrs., under constant stirring. The pH of the resulting solution was maintained between 9-10, using nitric acid and/or sodium hydroxide. The pH is maintained to get the desired hydrotalcite structure. The temperature of the mixture was then raised to 80 °C for 16 hrs., for aging. The resulting mixture was then cooled, filtered and washed using excess de-ionized water in batches to ensure complete removal of sodium and other impurities.

The catalyst was dried overnight at 70 °C and afterwards calcined at 600 °C for 6 hrs. The calcined catalysts were then pelletized to make size range of 75-150 µm.

3.2.2 Reduction and Passivation

The calcined catalysts were reduced and passivated in a fixed-bed quartz reactor. The reactor was fitted with a thermocouple to measure the inside temperature. The gases entered from the top of the reactor and left from the bottom.

3.2.3 Complications

During the hydrogen chemisorption for the NiCo-40 metal dispersion results were observed to be out of continuity as compared to rest of the hydrotalcite catalysts. Due to this problem a remake of the NiCo-40 was made, which will be called NiCo-40R. Although later on it was found that the problem with metal dispersion results was happening due to uncomplete reduction when performing the characterization. Some of the characterizations were carried out for the NiCo-40 remake catalyst. Which would be discussed in the results section of this report.

3.3 Catalyst Characterization

The synthesized hydrotalcite catalysts were analyzed with specialized equipment for certain catalytic properties. The details of the characterization procedures are given below.

3.3.1 X-ray fluorescence (XRF)

The x-ray spectra of the hydrotalcite catalysts were measured using Rigaku Supermini 200 unit. The sample was prepared by mixing 200 mg of catalyst weight with 3 g of boric acid. Boric acid acts as a binder, the mixture was then pelletized into a 30 mm disc to be used in the Rigaku

Supermini 200. The pellet covered with polypropylene film was placed in the sample holder and then placed in the equipment. The sample was then measured at 36.8 °C under 24.8 ml/min of P10 gas (10% methane in argon). X-ray tube implied a Pd-anode at 50 kV and 200 W.

3.3.2 Temperature programmed reduction

The temperature programmed reduction (TPR) profile spectra of the hydrotalcite catalysts were measured using an Altamira Benchcat Hybrid-1000HP unit. The samples were measured around 100 mg and placed inside a U-shaped quartz reactor between layers of quartz wool. A thermocouple was placed in the reactor to measure the temperature above the sample. The procedure was performed under 10 % hydrogen in argon flow. The sample was heated to 900 °C from ambient temperature ramping at 10 °C/min. The hydrogen consumption at the outlet was measured as a function of temperature using a thermal conductivity meter.

3.3.3 Hydrogen chemisorption

The hydrogen chemisorption of the hydrotalcite catalysts was carried out in a Micrometrics ASAP-2010 unit. A sample weight of 200 mg was measured and loaded in a U-shaped quartz reactor between two layers of quartz wool. The temperature of the reactor was measured using a thermocouple which was located outside the reactor adjacent to the sample. The sample was evacuated for 2 hours down to a pressure of 0.003 µmHg. The reactor was then leak checked to ensure that maximum pressure drop was less than 50 µmHg/min. the sample was heated by placing an electric furnace around the reactor. The experiment sequence, **Table 3.3**, was initiated after the successful completion of the leak test.

Table 3.3: Summary of hydrogen chemisorption sequence and conditions

Step	Name	Temperature [°C]	Rate [°C/minute]	Time [minutes]
1.	Evacuation	40	10	60
2.	Automatic Leak Test	40	10	--
3.	Hydrogen Flow	670	2	600
4.	Evacuation	670	2	30
5.	Evacuation	40	10	60
6.	Automatic Leak Test	40	10	--
7.	Evacuation	40	10	30
8.	Analysis	40	10	--

An adsorption isotherm was constructed using data points of quantity absorbed against pressure. The surface area and the dispersion was calculated using Equation (2.20) and Equation (2.21).

3.3.4 Nitrogen adsorption

The nitrogen adsorption of the hydrotalcite catalysts was performed in a Micrometrics TriStar 3000 unit. The process was carried out using up to 120 mg of hydrotalcite catalyst in a long necked quartz tube at the temperature of liquid nitrogen 196 °C. Before starting the experiment, the samples were degassed for 1 hour at room temperature followed by an overnight degassing at 200 °C.

The nitrogen adsorption isotherm was generated. BET surface area and other physical characteristics were calculated from the procedure mention in section **2.4.4**. Furthermore, pore-size distribution and pore volume was also calculated using the BJH method [5].

3.3.5 X-ray diffraction (XRD)

Bruker D8 Advance DaVinci Diffractometer was used to perform the x-ray diffraction analysis. The instrument uses CuKα radiation to obtain the XRD spectra. The samples were ground to a fine powder and added to sample holders for measurement. For the measurement, fixed angle at 0.4 degrees was chosen and the 2θ range was measured from 20° to 80° in 1 hour.

3.3.6 Transmission electron microscopy (TEM)

TEM samples were prepared by ultrasonic dispersion of the powdered sample in ethanol. Drops of dispersion were applied on a copper grid supported with a carbon film. TEM images were taken by a JEOL 2010F.

3.4 Kinetic analysis

The kinetic analysis of the hydrotalcite catalysts was performed in a fixed-bed reactor. The details of the setup and the experimental procedure follows.

3.4.1 Steam reforming setup

The steam methane reforming setup schematics are shown in **Figure 3.1**. The setup used for the steam reforming process was a custom made pilot plant manufactured by Process Integral Development Eng. & Tech. Some of the main features of the system included, independent gas and liquid feed, independent reactor temperature, independent pressure control and

independent L/G separator [35]. The setup implied Bronkhorst MFC for controlling mass flows, pressure and liquid level.

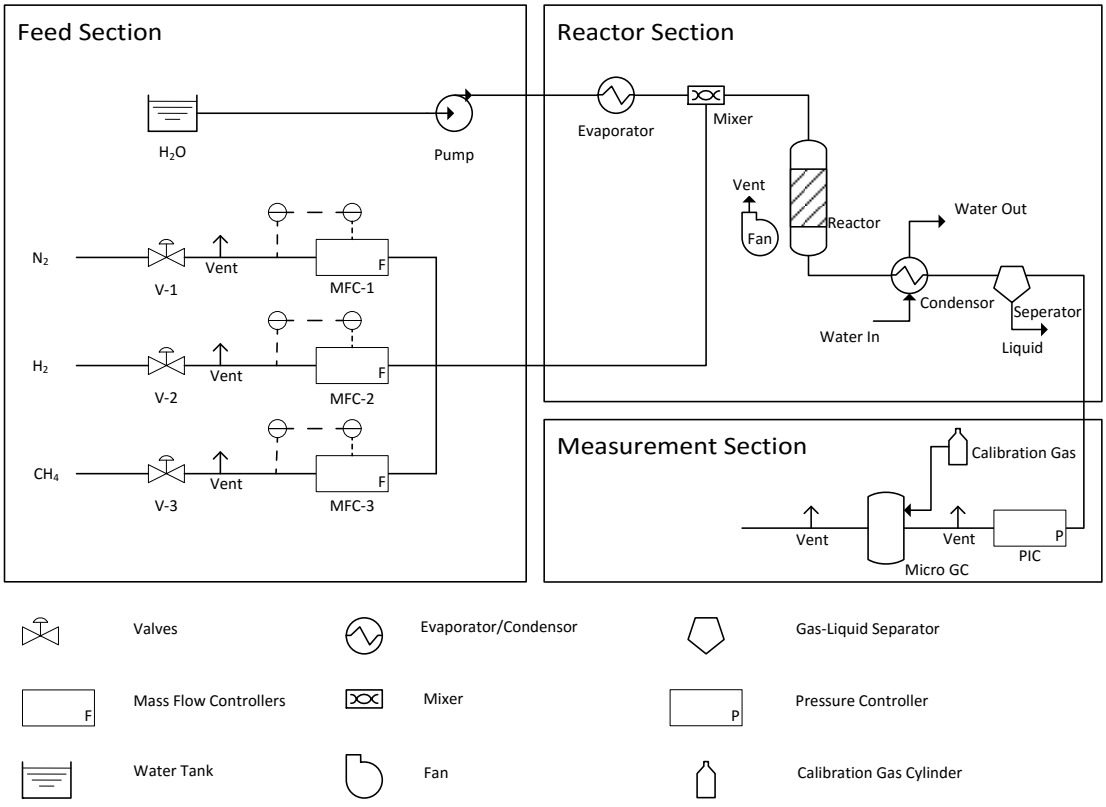

Figure 3.1: Schematic diagram of the steam reforming setup

In **Figure 4.1**, the reactor, thermocouple, mixer and the evaporator are all installed inside a hot box. Temperature sensors and a centrifugal fan are fitted inside the hot box to maintain desired temperature. The gaseous products from the reaction were analyzed using Agilent 3000 Micro GC. The data from the Agilent 3000 Micro GC was analyzed using Agilent Cerity Networked Data System.

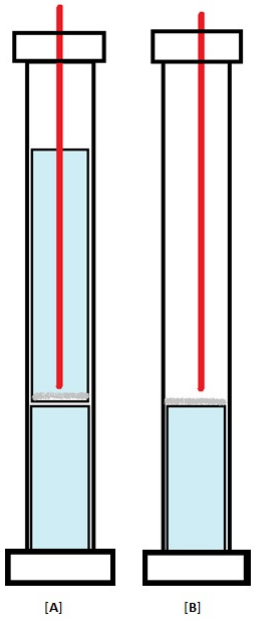

Figure 3.2: Different reactor configurations

As shown in **Figure 3.2**, a thermocouple is inserted in the reactor (shown in red), the reactor contains two internal removable cylinders of different lengths. There is a wire gauze on one end of the cylinders while the other end is open. The reactor functions with both cylinders, configuration A, or with only one cylinder, configuration B. In case of configuration A, both of the cylinders are placed end to end one over the other inside the reactor. The top cylinder is placed inverted over the bottom cylinder and the catalyst rests inside the top cylinder over a bed of alumina fibers. The thermocouple is inserted in to the top cylinder just above the catalyst. While in case of configuration B, only one of the cylinders is placed inside the reactor with the wire gauze side upwards. The catalyst is placed over the wire gauze on a bed of alumina fibers, the thermocouple is inside the reactor on the top of the cylinder just above the catalyst.

3.4.2 Steam reforming experiment

The standard configuration B was used for the kinetic analysis, and was selected based on the results explained in section **4.7.1**. The hydrotalcite catalysts were placed inside the reactor in configuration B, as explained in section **3.4.1**.

Before starting the experiment, a leak test was performed with hydrogen flow up to 135.5 ml/min. The reduction of the catalysts was carried out in-situ. After reduction, the reactor was cooled to prevent coke formation. Water flow was started and liquid level controller LIC 2 was monitored to be stable to start the methane flow. Hydrogen flow was maintained to keep the

catalysts in reduced state. The risk assessment for the steam reforming process is given in **Appendix B.**

3.5 Reaction conditions

Different reaction conditions were implied for kinetic analysis, and for the reaction order experiments. The details of the reaction conditions and physical properties of the catalysts are given below.

3.5.1 Reduction conditions

The reduction of the catalysts was carried out in-situ at 670 °C for 10 hours with a heating rate of 2 °C/min. The hydrogen to nitrogen ratio was maintained at 1:1 with both flows at 75 ml/min. After reduction the reactor was cooled down to the desired reaction temperature using a ramping rate of 2 °C/min.

3.5.2 Kinetic analysis conditions

The 15 mg of 75-150 micrometer hydrotalcite catalyst was used for the kinetic analysis. The catalyst was diluted using 150 mg of α-alumina of the same size.

The steam methane reforming reaction was carried out at 500 °C, 525 °C, 550 °C, 575 °C, and 600 °C. The pressure inside the reactor was maintained at 100 KPa. Hydrogen and methane flows were fixed at 75 ml/min and the water flow was set to 262.5 ml/min, thus maintaining the total flow at 409.5 ml/min and steam to carbon ratio at 3.5:1.

3.5.3 Methane pressure analysis conditions

The 10 mg of 75-150 micrometer hydrotalcite catalyst was used for the kinetic analysis. The catalyst was diluted using 100 mg of α-alumina of the same size.

The steam methane reforming reaction was carried out at 500 °C and 150 KPa. The total flow was set to 325 ml/min and steam to carbon ratio at 3.5:1. The methane partial pressure corresponding to the different flows for the methane pressure test are given in **Table 3.4**.

Table 3.4: Methane partial pressure corresponding to different flow rates for methane pressure test

Methane Partial Pressure [KPa]	**Methane Flow** [ml/min]	**Hydrogen Flow** [ml/min]	**Water Flow** [ml/min]	**Nitrogen Flow** [ml/min]
27.7	60	60	210	0
25.4	55	55	192.5	22.5
23.1	50	50	175	50
20.8	45	45	157.5	77.5
18.5	40	40	140	105

3.5.4 Water pressure analysis conditions

The 15 mg of 75-150 micrometer hydrotalcite catalyst was used for the kinetic analysis. The catalyst was diluted using 150 mg of α-alumina of the same size.

The steam methane reforming reaction was carried out at 550 °C and 100 KPa. Hydrogen and methane flows were fixed at 74 ml/min. The total flow was set to 400 ml/min. The water partial pressure corresponding to different water and nitrogen flows for the water pressure test are given in **Table 3.5**.

Table 3.5: Water partial pressures corresponding to different flow rates for water pressure test

Water Partial Pressure [KPa]	**Water Flow** [ml/min]	**Nitrogen Flow** [ml/min]
60	240	12
55	220	32
50	200	52
45	180	72
40	160	92
37.5	150	102

3.5.5 Hydrogen pressure analysis conditions

The 15 mg of 75-150 micrometer hydrotalcite catalyst was used for the kinetic analysis. The catalyst was diluted using 150 mg of α-alumina of the same size.

The steam methane reforming reaction was carried out at 550 and 100 KPa. Methane flows were fixed at 75 ml/min and the water flow was set to 262.5 ml/min. The total flow was set to

412.5 ml/min and steam to carbon ratio at 3.5:1. The hydrogen partial pressure corresponding to different hydrogen and nitrogen flows for the water pressure test are given in **Table 3.6**.

Table 3.6: Different flow rates for hydrogen pressure test

Hydrogen Partial Pressure [KPa]	**Hydrogen Flow** [ml/min]	**Nitrogen Flow** [ml/min]
18.2	75	0
15.8	65	10
13.3	55	20
10.9	45	30
8.5	35	40
6.1	25	50

4 Results and Discussion

4.1 X-Ray Fluorescence (XRF)

X-ray fluorescence is a characterization technique used for the quantitative analysis. In this technique the x-ray spectra of the samples are measured to determine the compositions. The detailed results of the analysis are given in **Appendix C**, **Table C.**. The comparison of metal loadings of actual and measured nickel and cobalt are given in **Table 4.1**.

Table 4.1: Metal loadings of Nickel (Ni) and Cobalt (Co), Calculated Vs. XRF

Catalyst	**Nickel Calculated** [wt. %]	**Nickel from XRF** [wt. %]	**Cobalt Calculated** [wt. %]	**Cobalt from XRF** [wt. %]	**Nickel to Cobalt ratio from XRF**
NiCo-10	3	1.4	7	3.3	0.42
NiCo-20	6	3.4	14	7.2	0.47
NiCo-30	9	5.4	21	11.5	0.47
NiCo-40	12	7.7	28	16.5	0.47

The values of measured metal loading against actual metal loading vary greatly. But the increasing trend for both nickel and cobalt content supports the formation of the desired catalysts.

It is believed that the difference in metal loading actual and that measured by XRF is due to the complex layered hydrotalcite structure, which makes it difficult to accurate data. Also the presence of carbon in the samples could lead to an inaccuracy in the measured data. Also, the XRF equipment has problem measuring carbon, which leads to variation in measured quantities of other elements as well. More accurate methods for quantitative measurement of the calcined samples could be combining XRF with XRD, or by the use of ICP-MS technique. ICP-MS would be a more reliable method for quantitative analysis since it can measure most metals and non-metals at low concentrations.

4.2 Temperature programmed reduction (TPR)

The activation of the hydrotalcite catalysts is studied in hydrogen atmosphere using temperature programmed reduction. The TPR profile spectra of the hydrotalcite catalysts is shown in **Figure 4.1**. In the data presented here, NiCo-40 refers to the remake of 40 % nickel cobalt hydrotalcite. The data was included because of the unavailability of TPR data for actual

NiCo-40 catalyst, as explained in section **3.2.3**, due to a technical problem with Benchcat Hybrid.

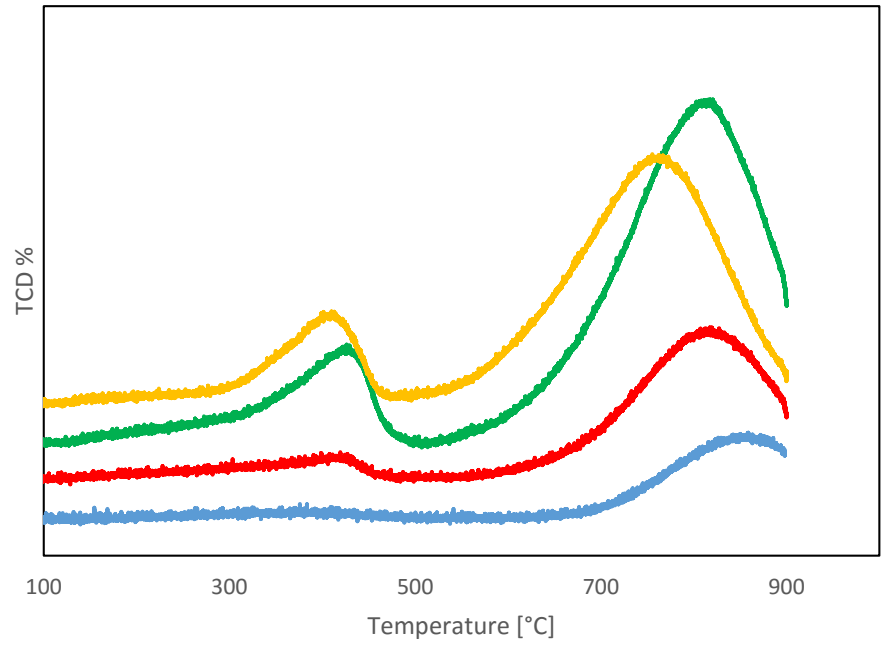

Figure 4.1: Temperature programmed reduction profiles for nickel-cobalt hydrotalcite catalysts up to a maximum temperature of 900 °C. —NiCo-10, —NiCo-20, —NiCo-30, —NiCo-40R

The first peak which occurs at 423 °C for all of the catalysts refers to the reduction of Co_3O_4 to CoO. There could be a fraction of the peak that also refers to the reduction of CoO to Co^0. The second peak, are actually two overlapping peaks which refers to the second step of reduction i.e. the reduction of CoO to Co^0 and the reduction of NiO to Ni. These results are in accordance with the results of previous studies [9]. Both peaks indicate a significant difficulty of reduction mainly pointing to the complex layered structure of hydrotalcites. This increased temperature is also much higher than for pure nickel and cobalt because of the strong interactions of pure nickel and cobalt with the support [9]. It is also evident from **Figure 4.1** that increasing loading shifts the first peak slightly to the right and the second peak slightly to the left, although this effect is not pronounced. It is also clear that the hydrogen uptake increases with increasing loading, other than the exception for NiCo-40 remake, but because of the unavailability of data for NiCo-40 this cannot be commented on.

4.3 Hydrogen chemisorption

The metal dispersion of the hydrotalcite catalysts was measured using hydrogen chemisorption. Chemisorption studies for bimetallic nickel-cobalt catalysts are complex and no standard

procedure is available to conduct the analysis. It is generally assumed that Nickel has zero activation energy for hydrogen adsorption and 300 K is the typical temperature required. Also, a significant kinetic barrier exits for the hydrogen adsorption for cobalt at low temperatures. The temperature required for hydrogen adsorption for cobalt is 400 K. Due to these reasons, certain difficulty exists in choosing an experimental temperature to establish monolayer adsorption on the surface of nickel-cobalt catalysts [9]. The results of the metal dispersion calculated from hydrogen chemisorption are given below in **Table 4.2**. The hydrogen chemisorption isotherms are given in **Appendix D**.

Table 4.2: Dispersion of NiCo hydrotalcite catalysts measured from hydrogen chemisorption

Catalyst	**Metal Dispersion** [%]	**Particle size from Metal Dispersion** [nm]
NiCo-10	4.9	19.9
NiCo-20	5.4	18.1
NiCo-30	5.6	17.7
NiCo-40	5.1	19.1

Metal dispersion is an important parameter in catalytic performance. The results indicate almost constant metal dispersion with increasing overall metal loading. In the previously conducted study, the metal dispersion was found to decrease with increasing cobalt loading for the hydrotalcite catalysts [8], this was explained due to the increased agglomeration of cobalt particles with increasing particle loading [9]. For 30% nickel and 70% cobalt the metal loading was 5% [8]. The results of hydrogen chemisorption are given in **Table 4.3**.

Table 4.3: Metal dispersion of calcined nickel-cobalt catalysts determined from hydrogen chemisorption [8]

Catalyst	**Metal Dispersion**
$\mathbf{Ni_{100}}$	9.9
$\mathbf{Ni_{70}Co_{30}}$	7.8
$\mathbf{Ni_{50}Co_{50}}$	6.0
$\mathbf{Ni_{30}Co_{70}}$	5.1
$\mathbf{Co_{100}}$	5.0

The metal dispersion for the hydrotalcite catalysts are all around 5 % which is in accordance with the previous results of 30% nickel and 70% cobalt hydrotalcite catalyst. This indicates the dependence of metal dispersion on nickel to cobalt ratio and not the overall metal loading. A

similar trend can be observed for the average particle diameter as shown in **Figure 4.2**. Evidently the particle size varies with varying metal dispersion.

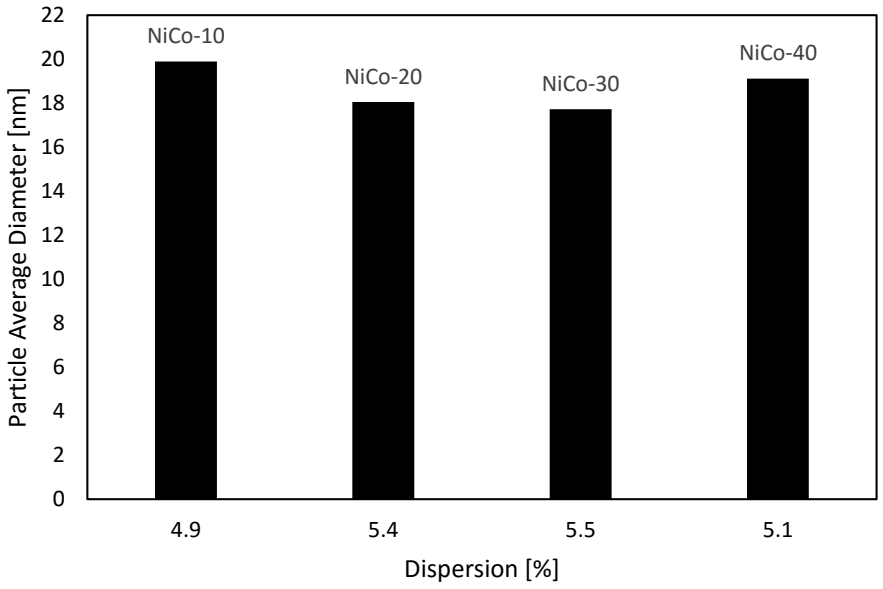

Figure 4.2: Variation of particle average diameter with metal dispersion

When analyzing the chemisorption isotherms for the hydrotalcite catalysts, it was found that the isotherm for the NiCo-10 shows an unusual behavior, as shown in **Appendix D**, **Figure D.1**. This behavior was inconsistent with the behavior of other isotherms and was not expected, although the metal dispersion results seemed promising. To investigate the behavior further the experiment was repeated but the isotherm results were almost the same. It is assumed that the inconsistency with the isotherm was due to technical issues with the instrument, because the catalyst otherwise behaved properly.

4.4 Nitrogen adsorption

The BET surface area and adsorption pore diameter in addition to metal dispersion and particle size is given in **Table 4.4**. the nitrogen adsorption and desorption isotherm plots are given in **Appendix E**. From the data in **Table 4.4**, it is clear that the BET surface area and the metal dispersion decreases with increasing overall metal loading while the average pore diameter and particle size remains almost constant.

Table 4.4: Nitrogen adsorption data for the hydrotalcite catalysts

Catalyst	BET Surface Area [m^2/g]	Average pore diameter [nm]
NiCo-10	169	9.07
NiCo-20	159	9.08
NiCo-30	138	9.36
NiCo-40	130	8.99

The adsorption isotherms shown in **Appendix E**, indicate type 2 adsorption isotherm [36]. Which means that the samples have a rather steep uptake at high relative pressure. Indicating that the hydrotalcite catalysts have larger pores and narrow pore size distribution [17].

4.5 Crystallite structure

Studying the x-ray diffraction spectra of a catalyst gives valuable insight about the structure, size and composition. For the purpose of this study, XRD is used to assess the structure of both calcined and uncalcined hydrotalcite catalysts. The x-ray powder diffraction profile spectra of the uncalcined hydrotalcite catalysts is shown in **Figure 4.3**, and for the calcined hydrotalcite catalysts **Figure 4.4** shows the XRD results.

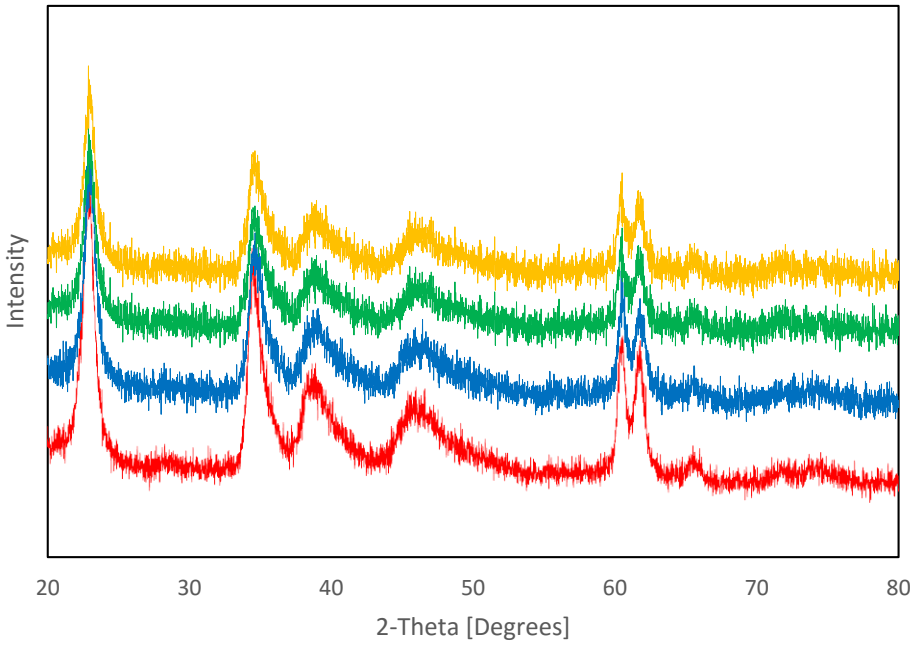

Figure 4.3: X-Ray powder diffraction profile spectra for uncalcined catalysts. —NiCo-10, —NiCo-20, —NiCo-30, —NiCo-40

The XRD profile for the uncalcined sample as shown in **Figure 4.3**, the peaks at 23°, 36°, 39°, 47°, 61° and 63° are clear and indicative of a typical hydrotalcite structure. These results are consistent with the studies conducted previously [12] [19], and confirm the formation of hydrotalcites.

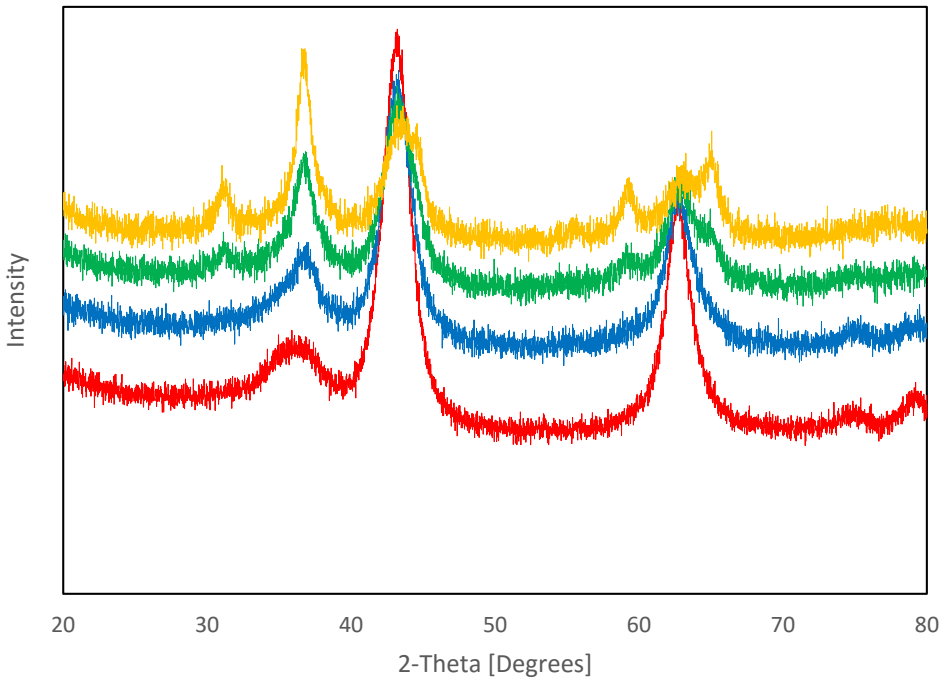

Figure 4.4: X-Ray powder diffraction profile spectra for calcined catalysts. —NiCo-10, —NiCo-20, —NiCo-30, —NiCo-40

In **Figure 4.4**, peaks observed at 37°, 43°, 63°, 75° and 79° are observed for all of the calcined hydrotalcite catalysts and confirm the formation of metal oxides. These peaks are in accordance with previously conducted studies on hydrotalcite catalysts [19] [35]. The peaks shown here for different components are overlapping and the phase identification is difficult. This relates to the fact that hydrotalcite being a very complex and layered structure is indistinguishable using XRD analysis. It has also been shown that because Ni^{+2}, Co^{+2} and Al^{+3} as Mg^{+2} have almost same crystallite size all of these will take similar lattice when put into solid solution and will not be separately identifiable using XRD [35].

4.6 Morphology of the hydrotalcite catalysts

The structural of the hydrotalcite catalyst as observed by TEM is shown in **Figure 4.5**.

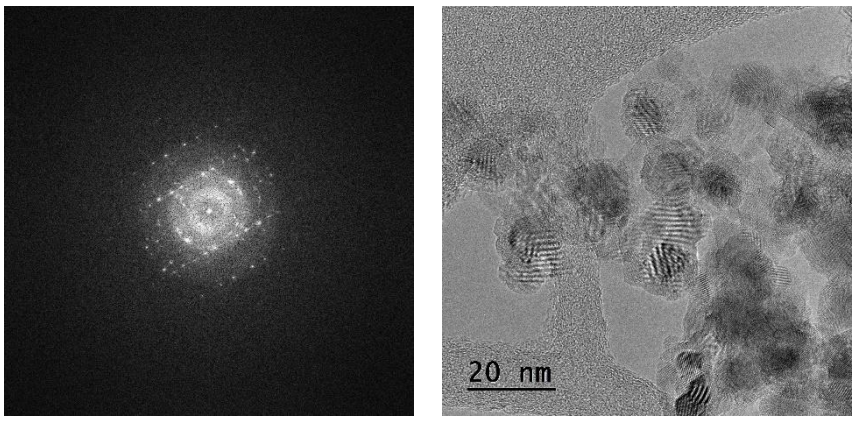

Figure 4.5: Structural morphology of the hydrotalcite catalysts as observed by transmission electron microscope, Single particle of NiCo-40 (Left), Particle cluster of NiCo-40 (Right)

In **Figure 4.5**, the structure of reduced and passivated NiCo-40 is observed using TEM. The image on the left shows the morphology of a single particle. The image on the right shows a more detailed view of a cluster of particles and a layered structure is visible which is indicated by the steps in the image. It is considered that the stepped structure is a result of the interactions between nickel and cobalt atoms. It is believed that since the nickel and cobalt crystals do not layer properly which gives rise to this stepped structure. This could be one of the reasons for the high activity of the nickel-cobalt catalysts as compared to pure nickel or cobalt based catalysts. The particle size as observed by the TEM is found out to be 10 nm, the layer around the particles refer to the passivation.

4.7 Kinetic Analysis

From now on the kinetic analysis of the hydrotalcite based catalysts would be discussed.

4.7.1 Mass transfer limitations

An analysis was conducted to analyze mass transfer limitations for previously made catalysts [8], using different reactor configurations and different catalyst sizes. The reactor configurations are discussed previously in section **3.4.1**. The results of the analysis are given in **Figure 4.6**.

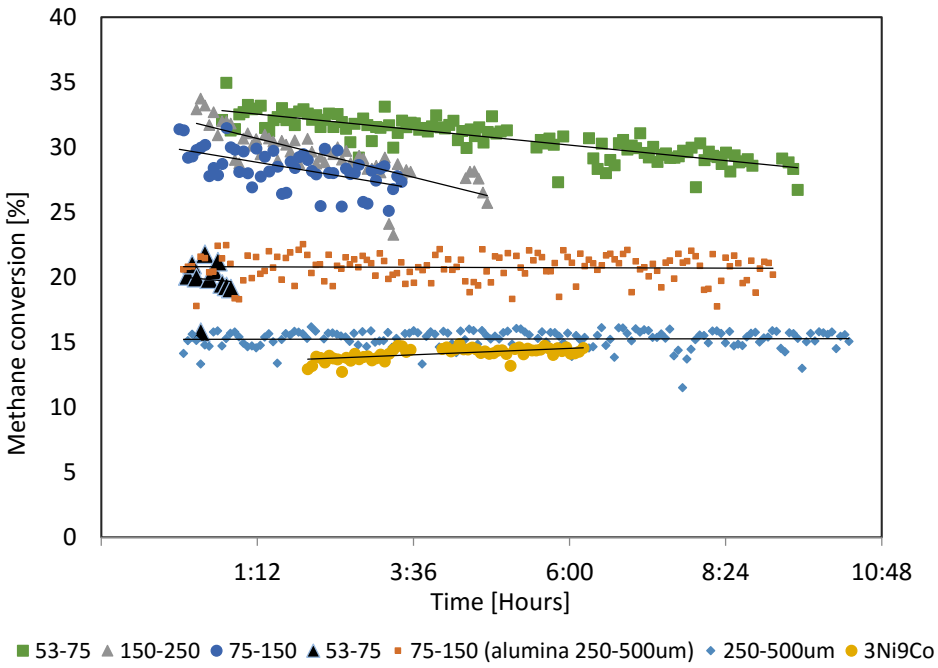

Figure 4.6: Analyzing mass transfer limitations for different reactor configurations and catalyst sizes, plots ■53-75 µm, ▲150-250 µm and ●75-150 µm are for reactor configuration B, while plot ▲53-75 µm, ■75-150 µm (alumina 250-500 µm), ◆250-500 µm and ●3 % Ni 9% Co are for reactor configuration A [36]

The top three plots for sizes ■53-75 µm, ▲150-250 µm and ●75-150 µm are for reactor configuration B, while plot ▲53-75 µm, ■75-150 µm (alumina 250-500 µm), ◆250-500 µm and ●3%Ni 9% Co are for reactor configuration A, as explained in section **3.4.1**. All of the plots are for 12% Ni except 3% Ni 9% Co which is sized 250-500 µm [36].

It can be seen that for reactor configuration B the methane conversion decreases over time and the catalysts are not stable. While it is clear that in the case of reactor configuration A all of the catalytic sizes yield stable methane conversion. On further investigation, pointed to the fact that for reactor configuration A, the catalyst was shielded by a double wall (one wall of the cylinder and one wall of the reactor) as shown in **Figure 3.2**. Due to this, the heat transfer from the furnace was reduced, thus reducing the amount of heat required for the best conversion possible. Moreover, it was also found out that the deactivation for reactor configuration B was not significant and conversion gained was also considerably higher as compared to reactor configuration A. It can also be seen that higher stability and methane conversion was observed for 53-75 and 75-150 micrometer particle size as compared to other particle sizes due to less mass transfer limitations. The size 75-150 micrometer was selected because of ease of use as compared to 53-75 micrometer.

For the purpose of this study, reactor configuration B was selected to be the default configuration to carry out all of the experimentation. Also, 75-150 micrometer was selected as the default size for the hydrotalcite catalysts and α- alumina which would be used as a diluting agent due to lesser mass transfer limitations in this size.

4.7.2 Methane conversion

One of the main consideration is given to methane conversion when studying the kinetics of steam methane reforming. Methane conversion variation at different temperatures and 100 kPa is studied using different hydrotalcite catalysts. The analysis conditions are given in section **3.5**, and the results are shown in **Figure 4.7**.

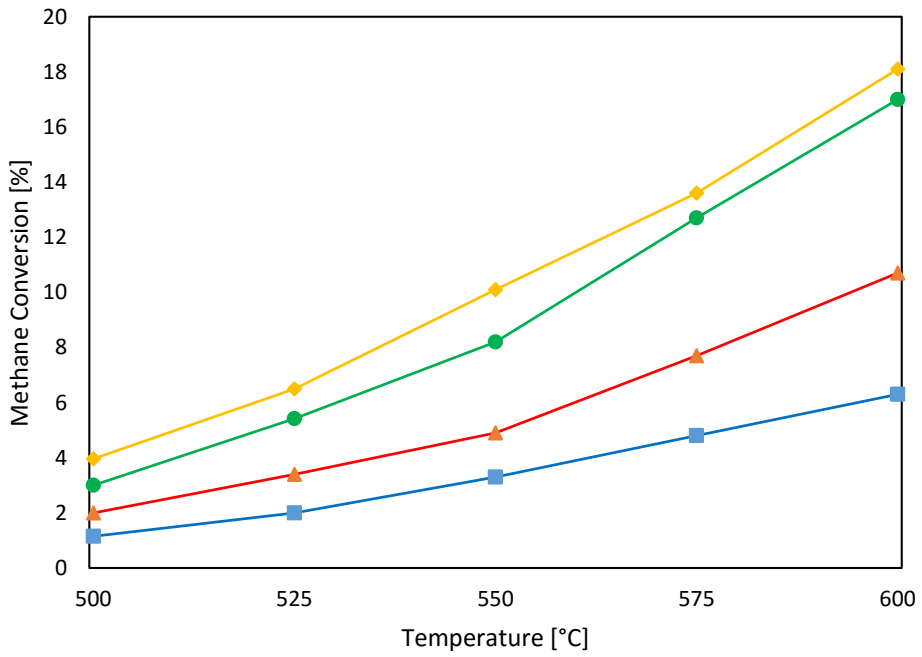

Figure 4.7: Effect of temperature on methane conversion for different catalysts at 500 °C, 525 °C, 550 °C, 575 °C, 600 °C and 100 kPa, the S:C ratio is 3.5:1. ■ NiCo-10, ▲ NiCo-20, ● NiCo-30, ◆ NiCo-40

From **Figure 4.7**, it can be seen that the methane conversion rises with rise in temperature from 500 °C and is maximum at 600 °C. All of the plots of methane conversion are concave upwards and an almost exponential increase can be observed after 550 °C. Minimum conversion of methane can be observed for NiCo-10 and maximum conversion is evident for NiCo-40. While methane conversions for NiCo-20 and NiCo-30 are in the intermediate range. This implies that the combination of nickel and cobalt in this ratio gives increasing conversion with increasing metal loading.

4.7.3 Turnover frequency

Catalytic Activity measured in terms of turnover frequency (TOF) which is defined as 'Number of molecules converted per active site per unit time'. The TOF of the catalysts is measured at different temperatures for the steam reforming of methane at a pressure of 100 KPa. The analysis conditions are given in section **3.5**, and the results are shown in **Figure 4.8**.

The variation of TOF at different temperatures is plotted against increasing metal loadings. It can be seen that at low temperatures TOF remains almost constant for all metal loadings. As the temperature is increased TOF is increased for NiCo-10 but it still remains constant for all other metal loadings. Previously [8], it was observed that TOF was maximum for 70% cobalt and 30% nickel. It was assumed, that in this ratio of nickel and cobalt, the catalysts exhibited maximum activity. And, that the rate determining step was being changed for the bimetallic hydrotalcite catalysts as compared to pure nickel or cobalt hydrotalcite catalysts. So to investigate the effect of increasing overall metal loadings this batch of catalysts was prepared with the same ratio of nickel and cobalt.

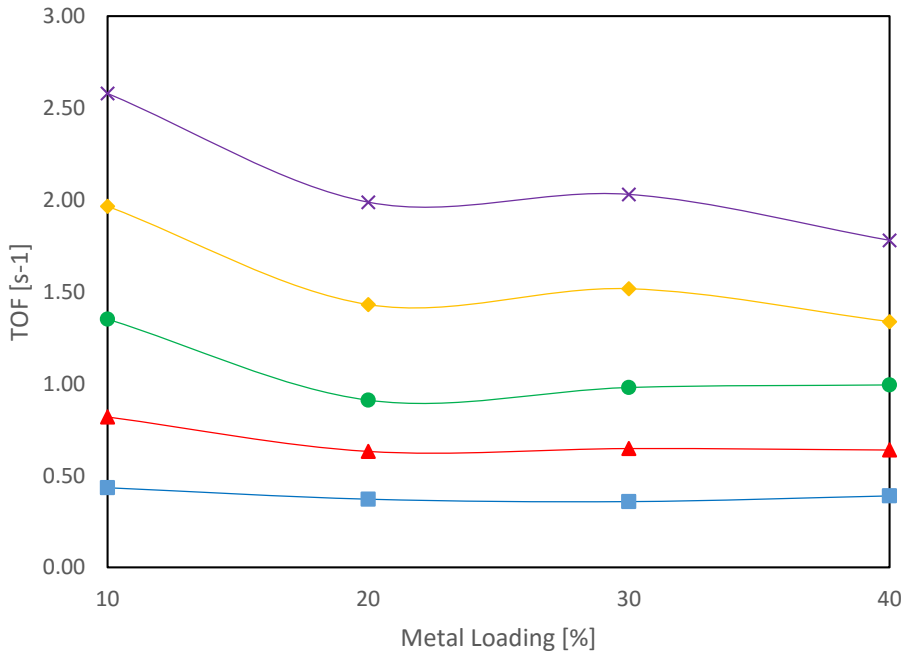

Figure 4.8: Effect of increasing metal loading on turnover frequency at 100 kPa, the S:C ratio is 3.5:1. ■ 500 °C, ▲ 525 °C, ● 550 °C, ◆ 575 °C and x 600 °C

In **Figure 4.9**, TOF is plotted against different temperatures for all of the hydrotalcite catalysts. the previous conclusion is again verified depicting the maximum activity for NiCo-10 while all of the other hydrotalcite catalysts have almost similar activity.

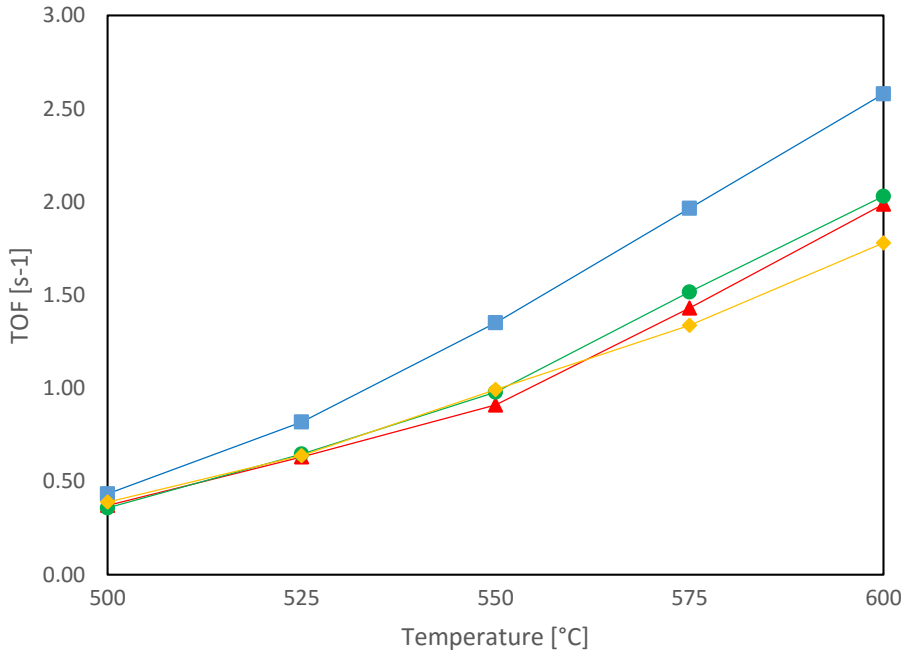

Figure 4.9: Variation of turnover frequency with temperature for hydrotalcite catalysts at 500 °C, 525 °C, 550 °C, 575 °C, 600 °C and 100 kPa, the S:C ratio is 3.5:1. ■ NiCo-10, ▲ NiCo-20, ● NiCo-30, ◆ NiCo-40

4.7.4 Rate of Reaction

The variation in rate of reaction with increasing metal loadings is plotted for different temperatures for the steam reforming of methane at a pressure of 100 KPa. The analysis conditions are given in section **3.5**, and the results are shown in **Figure 4.10**.

From **Figure 4.10**, it can be seen that the rate of reaction rises with rise in temperature from 500 °C and is maximum at 600 °C. All of the plots for rate of reaction indicate that rate increases with increasing metal loading from NiCo-10 and is maximum for NiCo-30 then it remains almost constant for NiCo-40. While NiCo-20 has an intermediate rate. The increase in reaction rate with temperature is due to the fact the reaction is endothermic.

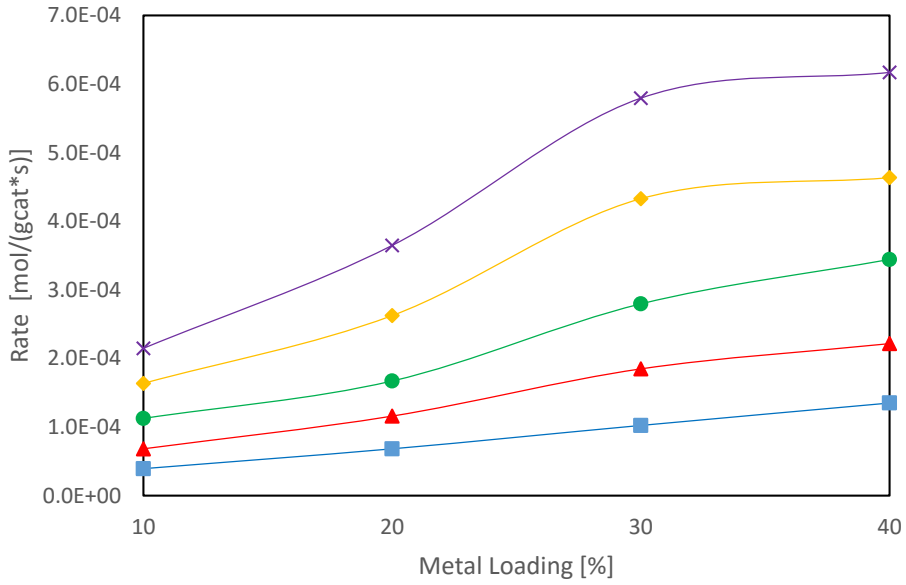

Figure 4.10: Effect of temperature on rate of reaction for hydrotalcite catalysts at 100 kPa, the S:C ratio is 3.5:1. ■ 500 °C, ▲ 525 °C, ● 550 °C, ◆ 575 °C and x 600 °C

4.7.5 Selectivity of carbon monoxide

The ability of a catalyst to direct a specific reaction to yield a particular product is the selectivity of a catalyst. Catalytic selectivity is an important catalyst parameter. The results for the carbon monoxide selectivity are shown in **Figure 4.11**. The analysis conditions are given in section **3.5**.

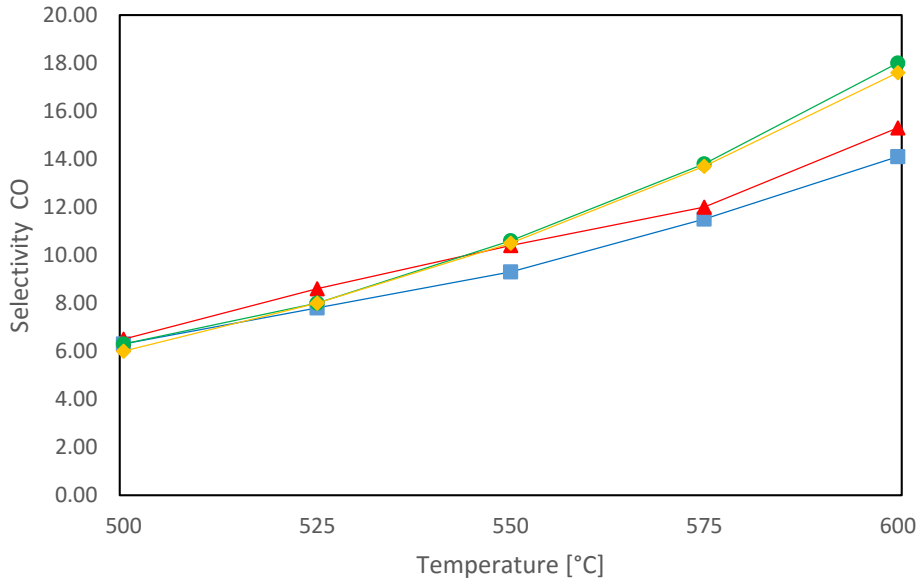

Figure 4.11: Variation of carbon monoxide selectivity with temperature at 500 °C, 525 °C, 550 °C, 575 °C, 600 °C and 100 kPa, the S:C ratio is 3.5:1. ■ NiCo-10, ▲ NiCo-20, ● NiCo-30, ◆ NiCo-40

In **Figure 4.11**, the average values of carbon monoxide selectivity are plotted against temperature for different hydrotalcite catalysts. The data suggest increase in carbon monoxide selectivity with increasing temperature, this is in accordance with the endothermic nature of the reaction. This implies the fact that steam reforming of methane is favored by high temperature, due to which the carbon monoxide production increases. Also WGS which consumes carbon monoxide is an exothermic reaction. Another important conclusion, that is drawn from the selectivity data is that selectivity for NiCo-30 and NiCo is almost same and quite high as compared to other catalysts above 550 °C. This is in accordance with the rate of reaction data as explained in **Section 4.7.4**, where it was represented that NiCo-30 and NiCo-40 had same rate of reaction.

4.7.6 Activation Energy

The effect of temperature is studied on steam reforming of methane using hydrotalcite catalysts. The reaction conditions are given in section **3.5**, and the results are given in the form of Arrhenius plot shown in **Figure 4.12**. The data shows that TOF increases with increasing temperature indicating overall forward reaction, this behavior is in accordance with Arrhenius type relation. A minor negative order of reaction is observed, but it is agreed upon that the reaction is first order with respect to methane.

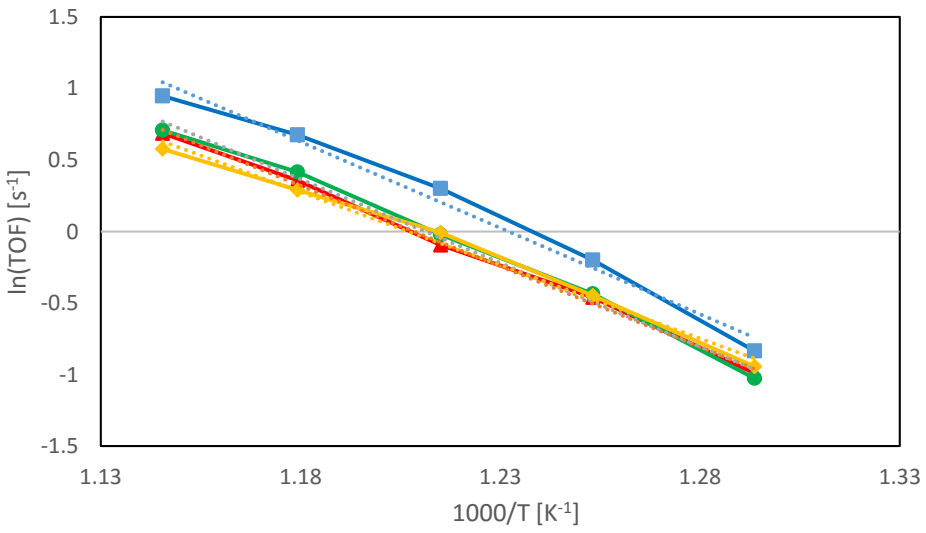

Figure 4.12: Arrhenius plot for hydrotalcite catalysts at 500 °C, 525 °C, 550 °C, 575 °C, 600 °C and 100 kPa, the S:C ratio is 3.5:1. ■ NiCo-10, ▲ NiCo-20, ● NiCo-30, ◆ NiCo-40

The activation energies and pre-exponential factors calculated from **Figure 4.12** are given in

Table 4.5. The order of decreasing activation energies is NiCo-10 > NiCo-30 > NiCo-20 > NiCo-40. It is apparent that the lowering of activation energy is the pronounced in case of NiCo-40, which indicates the effectivity of NiCo-40 for hydrogen production.

Table 4.5: Activation energies and pre-exponential factors calculated for hydrotalcite catalysts

Catalyst	**Activation Energy, Ea** [KJ/mol]	**Pre-exponential Factor, A** [s^{-1}]
NiCo-10	100.2	27.9 E+5
NiCo-20	93.8	8.3 E+5
NiCo-30	97.3	14.3 E+5
NiCo-40	84.9	1.7 E+5

4.7.7 Effect of methane, water and hydrogen pressure

The kinetic dependence of steam reforming of methane is studied on methane, water and hydrogen pressure, the results are shown in **Figure 4.13**, **Figure 4.14** and **Figure 4.15**. The conditions for the analysis are given in section **3.5**.

As shown in **Figure 4.13**, the rate of reaction for stem reforming of methane is plotted against methane partial pressure. The results indicate a linear increase in the reaction rate both for NiCo-10 and NiCo-40 which indicates dependency of the rate determining step on methane partial pressure indicating it to be firs order.

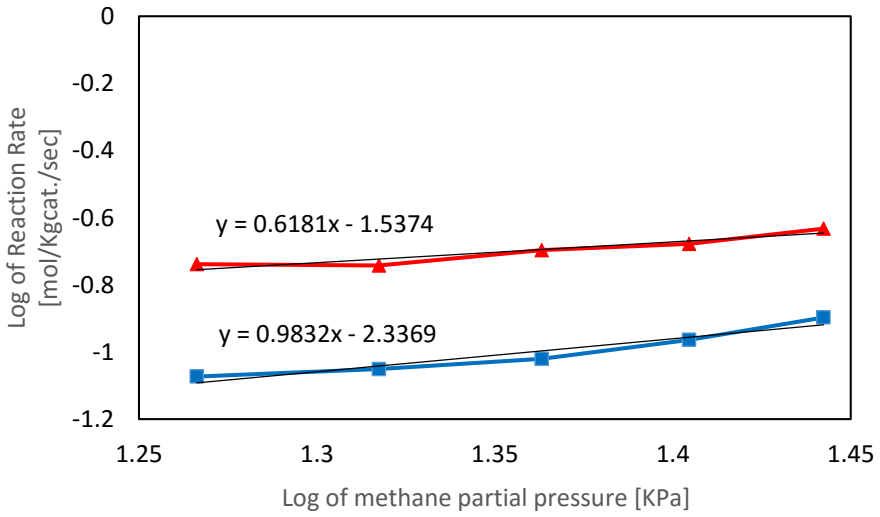

Figure 4.13: Variation of reaction rate with methane partial pressure at 550 °C and 100 KPa, total flow is 412.5 ml/min and S:C ratio is 3.5:1. ■ NiCo-10, ▲ NiCo-40

In **Figure 4.14**, reaction rate is plotted against water partial pressure, the plot shows a negative slope but the overall effect is almost constant and indicate no dependency on water partial pressure, for both hydrotalcite catalysts NiCo-10 and NiCo-40.

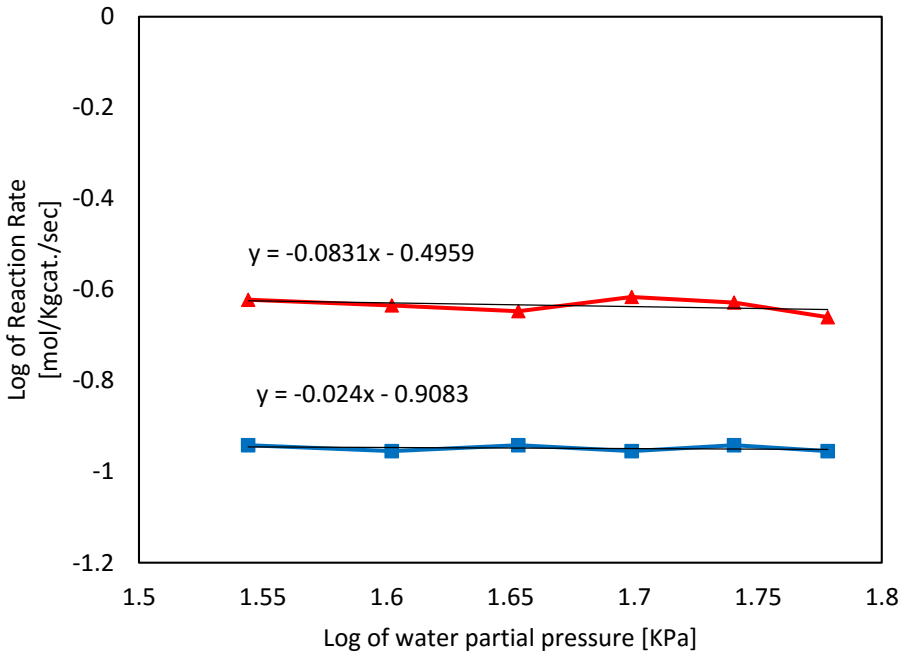

Figure 4.14: Variation of reaction rate with water partial pressure at 550 °C and 100 KPa, total flow is 400 ml/min. ■ NiCo-10, ▲ NiCo-40

The **Figure 4.15** shows the variation of reaction rate with hydrogen partial pressure. The data indicates that NiCo-10 is dependent on hydrogen partial pressure but the NiCo-40 does not appear to be dependent on hydrogen partial pressure. This could be an indication of change in mechanism due to increasing metal loading.

Methane conversion is also plotted against methane, water and hydrogen partial pressure. The results are given in **Appendix F**. The plots of methane forward conversion also verify the conclusion drawn in this discussion. Similar results have also been reported by Tayyaba Noor and Anh Hoang Dam in their respective doctoral dissertations [17] [19].

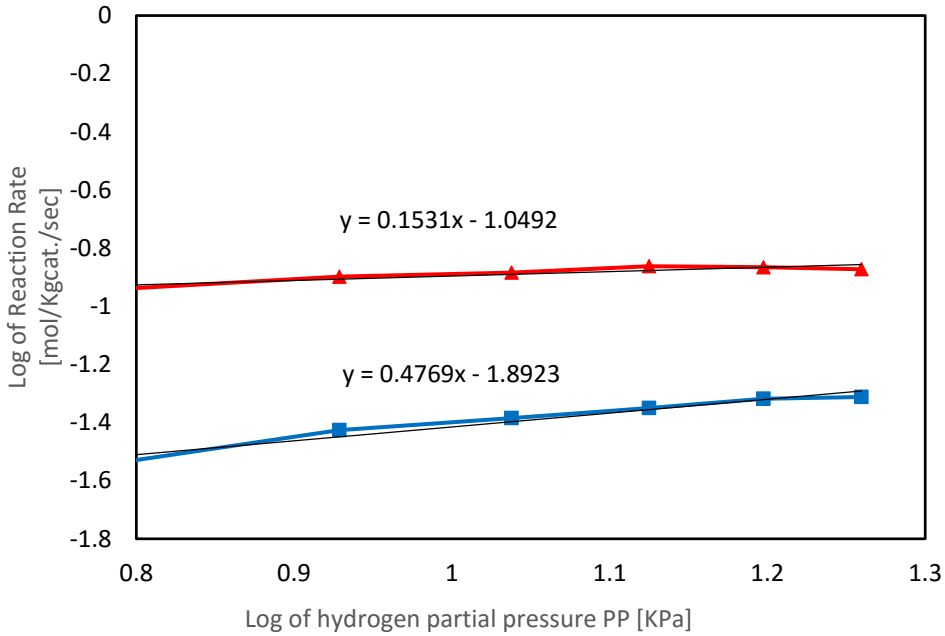

Figure 4.15: Variation of reaction rate with hydrogen partial pressure at 500 °C and 150 KPa, total flow is 325 ml/min and S:C ratio is 3.5:1. ■ NiCo-10, ▲ NiCo-40

5 Conclusion

The report in hand deals with the study of hydrotalcite based catalysts for the steam reforming of methane. Four nickel cobalt hydrotalcite catalysts were synthesized using the co-precipitation method. The nickel to cobalt ratio was kept fixed at 3:7 while the overall metal loading was increased from 10 wt.% to 40 wt.%. Some of the analysis like XRF, XRD, TPR, hydrogen chemisorption, nitrogen adsorption and kinetic analysis were carried out with calcined catalysts. While XRD and TEM analysis was carried out with reduced and passivated samples. For the purpose of kinetic analysis, a tubular fixed-bed reactor was implied.

The synthesis method used for the preparation of hydrotalcite catalysts was time consuming. But the characterization techniques show good results. Although XRF did not show exact composition of the catalysts, XRD succeeded in showing quite a lot of similarities with other hydrotalcite based studies. Similar similarities were also shown by hydrogen chemisorption, nitrogen adsorption and TEM analysis. It was seen that the metal dispersion results were as indicated by previously prepared samples in the same series. Also the dependency of the metal dispersion on nickel to cobalt ratio instead of the overall metal loading was also depicted. TEM analysis also indicated promising results, showing that the increased amount of step sites might be the reason the bimetallic catalysts shows such high activity. Nitrogen adsorption also showed high surface area and constant pore diameter.

The kinetic analysis represented some interesting facts about the nickel cobalt hydrotalcite catalysts. It was shown that the methane conversion increased with increased in temperature. Turnover frequency analysis indicated relatively constant activity other than for NiCo-10, while the highest rate of reaction was observed for NiCo-30 and NiCo-40. The selectivity data displayed that the water-gas-shift (WGS) was more pronounced at lower temperature, which was as expected. On the other hand, the reaction order tests indicated that the RDS depends on the methane partial pressure and that there might be a change in the reaction mechanism for NiCo-40, where it is also dependent on the hydrogen partial pressure.

Overall, it could be concluded that NiCo-10 was the most active catalyst based of the highest TOF. While, NiCo-30 is the most optimum hydrotalcite catalyst with respect to rate of reaction and selectivity. When taking into account the previously made catalysts it can also be said that; the mixed nickel cobalt hydrotalcite catalysts had much better activity and product selectivity as compared to pure nickel or pure cobalt hydrotalcite catalysts.

6 Future Research

Some of the future recommendations have been put together considering the promising data on hydrotalcite based materials for the steam reforming of methane.

First, the raw materials for the synthesis of nickel cobalt hydrotalcites need to be changed. This is because of the fact that the presence of any small amount of alkali based impurity (Na, K and/or Li) can poison the catalyst which makes it inactive. This can be achieved by implying ammonium hydroxide instead of sodium hydroxide in the synthesis process. Second, the co-precipitation process although having its benefits is a time consuming and complex process. The process needs to be optimized to reduce the synthesis time and also make it easier to upscale. Or some other method for the production of hydrotalcite catalysts can be investigated to reduce the complexity and time required.

For the hydrotalcite catalysts it is suggested that more detailed studies should be conducted to investigate the stability of the catalyst. Also, it has been found that cobalt enhances the activity of the nickel based hydrotalcite catalysts. More effort should be put into investigate the reason that why the activity is increased due to effect of cobalt. Another thing that could be done is to find more active combinations of nickel and cobalt for hydrotalcite catalysts.

One of the main problems that is faced industrially as well as on the lab scale is the coke formation. Not only coke formation increases the cost of the reaction but it also deactivates the catalyst. a study should be focused on investigating the coke formation mechanisms and reduction techniques for the nickel cobalt hydrotalcite catalysts.

7 Bibliography

[1] B. Petroleum, "Statistical Review of World Energy," [Online]. Available: http://www.bp.com/en/global/corporate/energy-economics/statistical-review-of-world-energy.html. [Accessed 15 7 2016].

[2] P. Häussinger, R. Lohmüller and A. M. Watson, "Hydrogen," in *Ullmann's Encyclopedia of Industrial Chemistry*, Wiley-VCH Verlag GmbH & Co., 2000.

[3] U. E. I. Administration, "The Impact of Increased Use of Hydrogen on Petroleum Consumption and Carbon Dioxide Emissions," [Online]. Available: http://www.eia.gov/oiaf/servicerpt/hydro/appendixc.html. [Accessed 15 July 2016].

[4] V. Tech, "Breakthrough in hydrogen fuel production could revolutionize alternative energy market," [Online]. Available: http://www.vtnews.vt.edu/articles/2013/04/040413-cals-hydrogen.html?utm_campaign=Argyle%2BSocial-2013-04&utm_content=shaybar&utm_medium=Argyle%2BSocial&utm_source=twitter&utm_term=2013-04-04-08-30-00. [Accessed 15 July 2016].

[5] G. Ertl, H. Knözinger, F. Schüth and J. Weitkamp, Eds., Handbook of Hetrogeneous Catalysis, vol. 1, Weinheim: Wiley-VCH Verlag GmbH& Co., 2008.

[6] I. Chorkendorff and J. W. Niemantsverdriet, Concepts of Modern Catalysis and Kinetics, Weinheim: WILEY-VCH Verlag GmbH & Co. KGaA, 2003.

[7] R. Salomão, L. M. Milena, M. H. Wakamatsu and V. C. Pandolfelli, "Hydrotalcite synthesis via co-precipitation reactions using MgO and Al(OH)3 precursors," *Ceramics International*, vol. 37, no. 8, pp. 3063-3070, December, 2011.

[8] S. E. Liland, B. Yousaf, Y. Wang, K. R. Raut and D. Chen, *Unprecedented Active and Stable Ni-Co Bimetallic Catalyst for Steam Methane Reforming*, Beijing: ICC, 2016.

[9] L. He, H. Berntsen, E. O. Fernández, J. C. Walmsley, E. A. Blekkan and D. Chen, "Co–Ni Catalysts Derived from Hydrotalcite-Like Materials for Hydrogen Production by Ethanol Steam Reforming," *Topics in Catalysis,* vol. 52, no. 3, pp. 206-217, April 2009.

[10] G. De Souza, V. C. Ávila, N. R. Marcílio and O. W. Perez-Lopez, "Synthesis Gas Production by Steam Reforming of Ethanol over M-Ni-Al Hydrotalcite-type Catalysts; M=Mg, Zn, Mo, Co," *Procedia Engineering,* vol. 42, pp. 1805-1815, 2012.

[11] F. Zhang, X. Xiang, F. Li and X. Duan, "Layered Double Hydroxides as Catalytic Materials: Recent Development," *Catalysis Surveys from Asia,* vol. 12, no. 4, pp. 253-265, December 2008.

[12] L. Bian, W. Wang, R. Xia and Z. Li, "Ni-based catalyst derived from Ni/Al hydrotalcite-like compounds by the urea hydrolysis method for CO methanation," *RSC Advances,* no. 1, pp. 677-686, December 2015.

[13] K. TakehiraAffiliated and T. Shishido, "Preparation of supported metal catalysts starting from hydrotalcites as the precursors and their improvements by adopting “memory effect”," *Catalysis Surveys from Asia,* vol. 11, no. 1, pp. 1-30, June 2007.

[14] F. Cvani, F. Trifirò and A. Vaccari, "Hydrotalcite-type anionic clays: Preparation, properties and applications.," *Catalysis Today,* vol. 11, no. 2, pp. 173-301, December 1991.

[15] S. Liu, D. Chen, K. Zhang, J. Li and N. Zhao, "Production of hydrogen by ethanol steam reforming over catalysts from reverse microemulsion-derived nanocompounds," *International Journal of Hydrogen Energy*, vol. 33, no. 14, p. 3736–3747, July 2008.

[16] J. A. Moulijn, M. Makkee and A. E. Van Diepen, Chemical Process Technology, West Susssex: John Wiley & Sons Ltd., 2013.

[17] T. Noor, "Sorption Enhanced High Temperature Water Gas Shift Reaction: Materials and Catalysis," NTNU, Trondheim, 2013.

[18] L. He, "Sorption Enhanced Steam Reforming of Biomass Derived Compounds: Process and Material," NTNU, Trondheim, 2010.

[19] A. H. Dam, "Bimetallic catalyst system for steam reforming," NTNU, Trondheim, 2015.

[20] J. A. Schwarz, C. Contescu and A. Contescu, "Methods for Preparation of Catalytic Materials," *Chem. Rev.*, vol. 95, pp. 477-510, 1995.

[21] L. . d. Viguerie, V. A. Sole and P. Walter, "Multilayers quantitative X-ray fluorescence analysis applied to easel paintings," *Anal Bioanal Chem (2009)*, 2009.

[22] Rigaku, "X-ray fluorescence," [Online]. Available: http://www.rigaku.com/en/techniques/xrf. [Accessed 19 December 2015].

[23] P. A. Webb and C. Orr, "Micrometrics," [Online]. Available: http://www.micromeritics.com/Repository/Files/Modern_Methods_of_Particle_Characterization.pdf. [Accessed 1 November 2015].

[24] "BET Theory," Wikipedia, [Online]. Available: https://en.wikipedia.org/wiki/BET_theory. [Accessed 1 November 2015].

[25] G. Ertl, H. Knozinger and J. Weitkamp, Eds., Handbook of Heterogeneous Catalysis, Weinheim: Wiley-VCH, 1997, pp. 427-582.

[26] M. I. Corporation, "Gas Adsorption Theory, Poster," [Online]. Available: http://www.micromeritics.com/Repository/Files/Gas_Adsorption_Theory_poster.pdf. [Accessed 23 July 2016].

[27] "Barrett-Joyner-Halenda (BJH) Analysis," Hiden Isochema, [Online]. Available: http://www.hidenisochema.com/glossary/65-barrett_joyner_halenda_(bjh)_analysis/. [Accessed 23 July 2016].

[28] "X-ray crystallography," Wikipedia, [Online]. Available: https://en.wikipedia.org/wiki/X-ray_crystallography. [Accessed 1 November 2015].

[29] J. W. Niemantsverdriet, Spectroscopy in Catalysis, Weinheim: WILEY-VCH, 2007.

[30] "Transmission electron microscopy," Wikipedia, [Online]. Available: https://en.wikipedia.org/wiki/Transmission_electron_microscopy. [Accessed 29 October 2015].

[31] "https://en.wikipedia.org/wiki/Matter_wave," Wikipedia, [Online]. Available: https://en.wikipedia.org/wiki/Matter_wave. [Accessed 31 October 2015].

[32] in *Industrial Catalysis: A Practical Approach*, Second, ed., Weinheim, WILEY-VCH Verlag GmbH & Co. KGaA , 2006.

[33] H. M. McNair and J. M. Miller, Basic Gas Chromatography, John Wiley & Sons, Inc., 1998.

[34] M. Trépanier, A. Tavasoli, A. K. Dalai and N. Abatzoglou, "Co, Ru and K loadings effects on the activity and selectivity of carbon nanotubes supported cobalt catalyst in Fischer–Tropsch synthesis," *Applied Catalysis A: General*, vol. 353, no. 2, pp. 193-202, 2009.

[35] H. Long, Y. Xu, X. Zhang, S. Hu, S. Shang, Y. Yin and X. Dai, "Ni-Co/Mg-Al catalyst derived from hydrotalcite-like compound prepared by plasma for dry reforming of methane," *Journal of Energy Chemistry*, vol. 22, p. 733–739, 2013.

Appendix A

Calculation of amount of reactant for different nickel-cobalt hydrotalcite catalysts

Nickel and Cobalt hydrotalcite contains CoO/NiO/MgO/Al_2O_3 after calcination which were converted to Co/Ni/MgO/Al_2O_3 after reduction. The compositions are determined as follows:

Let,

$$q = moles\ of\ Co, x = moles\ of\ Ni, y = moles\ of\ MgO\ and\ z = moles\ of\ Al_2O_3$$

The molar relationship is,

$$\frac{z}{q + x + y + z} = 0.25 \tag{A.1}$$

Weight fractions W_{Ni} and W_{Co} of nickel and cobalt respectively are given as,

$$W_{Ni} = \frac{M_{Ni}x}{M_{Co}q + M_{Ni}x + M_{MgO}y + M_{Al_2O_3}z} \tag{A.2}$$

And,

$$W_{Co} = \frac{M_{Co}q}{M_{Co}q + M_{Ni}x + M_{MgO}y + M_{Al_2O_3}z} \tag{A.3}$$

Now 3 equations have been set up for 4 unknowns. By setting z=1 the ionic relationships could be found out,

$$\frac{1}{q + x + y + 1} = 0.25 \Rightarrow y = 3 - x - q \tag{A.4}$$

Inserting Equation (A.4) into Equation (A.2) gives,

$$x = \frac{W_{Ni}\left(M_{Co}q - M_{MgO}q + 3M_{MgO} + {}^1\!/_2\, M_{Al_2O_3}\right)}{(1 - W_{Ni})M_{Ni} + W_{Ni}M_{MgO}} \tag{A.5}$$

Putting the values of x, y and z in Equation (A.3),

$$q = \frac{3M_{MgO} + {}^1\!/_2\, M_{Al_2O_3}}{\frac{M_{Co}}{W_{Co}}\left[(1 - W_{Ni}) + W_{Ni}\frac{M_{MgO}}{M_{Ni}}\right] - M_{Co} + M_{MgO}} \tag{A.6}$$

From here relationship for different catalysts is obtained,

Table A.1: Relationship coefficients for hydrotalcite catalysts

Catalyst	Weight fraction		Relative Numbers			
	W_{Ni}	W_{Co}	q	x	y	z
NiCo-10	0.03	0.07	0.21	0.09	2.70	1
NiCo-20	0.06	0.14	0.44	0.19	2.38	1
NiCo-30	0.09	0.21	0.68	0.29	2.03	1
NiCo-40	0.12	0.28	0.93	0.40	1.66	1

Since Al_2O_3 have 2 Al^{+3} ions and the requirement is to have an excess of CO_3^{-2} anion, the stoichiometric coefficients become,

Table A.2: Stoichiometric coefficients for hydrotalcite catalysts

Catalyst	Stoichiometric coefficients					
	Ni^{+2}	Co^{+2}	Mg^{+2}	Al^{+3}	OH^-	CO_3^{-2}
NiCo-10	0.18	0.42	5.40	2	16	1.5
NiCo-20	0.38	0.87	4.75	2	16	1.5
NiCo-30	0.58	1.35	4.06	2	16	1.5
NiCo-40	0.80	1.87	3.33	2	16	1.5

Molar mass for the reactants,

Table A.3: Molar mass for the reactants

Reactants	Molar Mass [g/mol]
$Ni(NO_3)_2.6H_2O$	298.81
$Co(NO_3)_2.6H_2O$	291.03
$Mg(NO_3)_2.6H_2O$	256.40
$Al(NO_3)_3.9H_2O$	375.13
NaOH	40.0
Na_2CO_3	105.99

Table A.4: Amounts of components in all the prepared catalysts

Catalyst	$Al(NO_3)_3.9H_2O$ [g]	$Mg(NO_3)_2.6H_2O$ [g]	$Co(NO_3)_2.6H_2O$ [g]	$Ni(NO_3)_2.6H_2O$ [g]	Na_2CO_3 [g]	NaOH [g]
NiCo-10	28.13	51.89	4.60	2.03	5.96	24
NiCo-20	28.13	45.70	9.51	4.20	5.96	24
NiCo-30	28.13	39.08	14.77	6.52	5.96	24
NiCo-40	28.13	31.98	20.40	9.01	5.96	24

Appendix B

Risk Assessment for steam reforming setup

ID	2783	**Status**	**Date**
Risk Area	Risikovurdering: Helse, miljø og sikkerhet (HMS)	Created	21.12.2015
Created by	Cristian Ledesma Rodriguez	Assessment started	21.12.2015
Responsible	Bilal Yousaf	Actions decided	
		Closed	

Master - Catalysis, 2015, Bilal Yousaf

Valid from-to date:

10/1/2015 - 7/1/2016

Location:

3 - Gløshaugen / 315 - Kjemi 5

Goal / purpose

This risk assessment contains all the activities that the master student Bilal Yousaf will perform in the labs of the Catalysis group.

Background

- Furnace
- Gas distribution system/cylinders
- Use of aluminium, cobalt and nickel precursors
- Use of acidic and basic solutions
- Stainless steel reactor

Summary, result and final evaluation

The summary presents an overview of hazards and incidents, in addtition to risk result for each consequence area.

Hazard:	**Use of high temperature furnaces**		
Incident:	**Electric shock**		
Consequence area:	Helse	Risk before actions:	Risiko after actions:
	Ytre miljø	Risk before actions:	Risiko after actions:
	Materielle verdier	Risk before actions:	Risiko after actions:
Incident:	**Uncontrolled heating**		
Consequence area:	Helse	Risk before actions:	Risiko after actions:
	Ytre miljø	Risk before actions:	Risiko after actions:
	Materielle verdier	Risk before actions:	Risiko after actions:
Incident:	**Fire**		
Consequence area:	Helse	Risk before actions:	Risiko after actions:
	Ytre miljø	Risk before actions:	Risiko after actions:
	Materielle verdier	Risk before actions:	Risiko after actions:

Incident: **Burn damage**

Consequence area:		
	Helse	Risk before actions: Risiko after actions:
	Ytre miljø	Risk before actions: Risiko after actions:
	Materielle verdier	Risk before actions: Risiko after actions:

Hazard: **Use of compressed gases (He,Ar)**

Incident: **Uncontrolled expansion and depleiton of O2**

Consequence area:		
	Helse	Risk before actions: Risiko after actions:
	Ytre miljø	Risk before actions: Risiko after actions:
	Materielle verdier	Risk before actions: Risiko after actions:

Incident: **Gas leakage**

Consequence area:		
	Helse	Risk before actions: Risiko after actions:
	Ytre miljø	Risk before actions: Risiko after actions:
	Materielle verdier	Risk before actions: Risiko after actions:

Hazard: **Use of aluminium, cobalt and nickel precursors**

Incident: **Spills on skin**

Consequence area:		
	Helse	Risk before actions: Risiko after actions:
	Ytre miljø	Risk before actions: Risiko after actions:
	Materielle verdier	Risk before actions: Risiko after actions:

Hazard: **Use of flammable gases (CH4,H2)**

Incident: **Fire, explosion**

Consequence area:		
	Helse	Risk before actions: Risiko after actions:
	Ytre miljø	Risk before actions: Risiko after actions:
	Materielle verdier	Risk before actions: Risiko after actions:

Incident: **Inhalation/Leakage**

Consequence area:		
	Helse	Risk before actions: Risiko after actions:
	Ytre miljø	Risk before actions: Risiko after actions:
	Materielle verdier	Risk before actions: Risiko after actions:

Hazard:	**Use of acetone for cleaning**		
Incident:	**Spills on skin**		
Consequence area:	Helse	Risk before actions:	Risiko after actions:
	Ytre miljø	Risk before actions:	Risiko after actions:
	Materielle verdier	Risk before actions:	Risiko after actions:

Hazard:	**Grinding and sieving of catalytic samples**		
Incident:	**Inhaling of harmful particles**		
Consequence area:	Helse	Risk before actions:	Risiko after actions:
	Ytre miljø	Risk before actions:	Risiko after actions:
	Materielle verdier	Risk before actions:	Risiko after actions:

Units this risk assessment spans

- Institutt for kjemisk prosessteknologi

Participants

Karin Wiggen Dragsten
Cristian Ledesma Rodriguez
De Chen
Shirley Elisabeth Liland

Readers

[Ingen registreringer]

Others involved/stakeholders

[Ingen registreringer]

The following accept criteria have been decided for the risk area Risikovurdering: Helse, miljø og sikkerhet (HMS):

Helse	Materielle verdier	Omdømme	Ytre miljø
			

Overview of existing relevant measures which have been taken into account for this risk assessment

The table below presents existing measures which have been take into account when assessing the likelihood and consequence of relevant incidents.

Hazard	Incident	Mesaures taken into account
Use of high temperature furnaces	Electric shock	HSE documentation
	Electric shock	Working alone regulations at NTNU
	Electric shock	Personal protective equipment
	Uncontrolled heating	HSE documentation
	Uncontrolled heating	Working alone regulations at NTNU
	Uncontrolled heating	Personal protective equipment
	Fire	HSE documentation
	Fire	Working alone regulations at NTNU
	Fire	Personal protective equipment
	Fire	Ventilation
	Fire	Gas detectors
	Burn damage	HSE documentation
	Burn damage	Working alone regulations at NTNU
	Burn damage	Personal protective equipment
	Burn damage	Ventilation
Use of compressed gases (He,Ar)	Uncontrolled expansion and depleiton of O2	HSE documentation
	Uncontrolled expansion and depleiton of O2	Working alone regulations at NTNU
	Uncontrolled expansion and depleiton of O2	Personal protective equipment
	Uncontrolled expansion and depleiton of O2	Ventilation
	Uncontrolled expansion and depleiton of O2	Leak test procedure
	Uncontrolled expansion and depleiton of O2	Installation and change of gas cylinders
	Gas leakage	HSE documentation
	Gas leakage	Working alone regulations at NTNU
	Gas leakage	Personal protective equipment
	Gas leakage	Ventilation
	Gas leakage	Leak test procedure
	Gas leakage	Installation and change of gas cylinders
Use of aluminium, cobalt and nickel precursors	Spills on skin	HSE documentation
	Spills on skin	Working alone regulations at NTNU
	Spills on skin	Personal protective equipment

Use of aluminium, cobalt and nickel precursors	Spills on skin	Ventilation
Use of flammable gases (CH4,H2)	Fire, explosion	HSE documentation
	Fire, explosion	Working alone regulations at NTNU
	Fire, explosion	Personal protective equipment
	Fire, explosion	Ventilation
	Fire, explosion	Gas detectors
	Fire, explosion	Leak test procedure
	Fire, explosion	Installation and change of gas cylinders
	Inhalation/Leakage	HSE documentation
	Inhalation/Leakage	Working alone regulations at NTNU
	Inhalation/Leakage	Personal protective equipment
	Inhalation/Leakage	Ventilation
	Inhalation/Leakage	Gas detectors
	Inhalation/Leakage	Leak test procedure
	Inhalation/Leakage	Installation and change of gas cylinders
Use of acetone for cleaning	Spills on skin	HSE documentation
	Spills on skin	Working alone regulations at NTNU
	Spills on skin	Personal protective equipment
Grinding and sieving of catalytic samples	Inhaling of harmful particles	HSE documentation
	Inhaling of harmful particles	Working alone regulations at NTNU
	Inhaling of harmful particles	Personal protective equipment

Existing relevant measures with descriptions:

HSE documentation

The laboratories have an updated Room Card and the unit 2.4 has a copy of the risk assessment, operating instructions and apparatus card with information regarding safety and information in case of emergency stop.

Different phone numbers are provided to contact in case of emergency.

Working alone regulations at NTNU

NTNU students and employee are not allowed to work alone after 7pm and during the weekends.

Working after 19:00 or in the weekends, you need to be at least 2 in the lab or in the building with regularly check-ups (every 30 minutes). Both of the people needs to have access to the labs

Personal protective equipment

The hall contains googles, other safety measures and a first-aid kit.. There are also gloves, lab coats and more protective equipment available upon request.

Ventilation

The reactor system is installed inside a cabinet with ventilation.

Gas detectors

The cabinet 2.2/2.3 in Chemistry Hall D has CO/H2, CH4/H2 and hydrocarbon detectors which will trigger the alarms in case of leakage. There are portable detectors that must be used during the leak tests before running experiments.

Leak test procedure

Before running experiments, a leak test must be performed following the procedure attached.

Installation and change of gas cylinders

This will be done by authorized personnel only.

Risk analysis with evaluation of likelyhood and consequence

This part of the report presents detailed documentation of hazards, incidents and causes which have been evaluated. A summary of hazards and associated incidents is listed at the beginning.

The following hazards and incidents has been evaluated in this risk assessment:

- **Use of high temperature furnaces**
  - Electric shock
  - Uncontrolled heating
  - Fire
  - Burn damage
- **Use of compressed gases (He,Ar)**
  - Uncontrolled expansion and depleiton of O2
  - Gas leakage
- **Use of aluminium, cobalt and nickel precursors**
  - Spills on skin
- **Use of flammable gases (CH4,H2)**
  - Fire, explosion
  - Inhalation/Leakage
- **Use of acetone for cleaning**
  - Spills on skin
- **Grinding and sieving of catalytic samples**
  - Inhaling of harmful particles

Overview of risk mitigating actions which have been decided, with description:

Use of high temperature furnaces (hazard)

Use of high temperature furnaces/Electric shock (incident)

Overall assessed likelihood of the incident: Less likely (2)

Comment to likelihood assessment:

[Ingen registreringer]

Assessment of risk for the consequence area: Helse

Assessed likelihood (common for incident): Less likely (2)

Assessed consequence: Medium (2)

Comment to consequence assessment:

[Ingen registreringer]

Use of high temperature furnaces/Uncontrolled heating (incident)

Overall assessed likelihood of the incident: Less likely (2)

Comment to likelihood assessment:

[Ingen registreringer]

Assessment of risk for the consequence area: Helse

Assessed likelihood (common for incident): Less likely (2)

Assessed consequence: Small (1)

Comment to consequence assessment:

[Ingen registreringer]

Use of high temperature furnaces/Fire (incident)

Overall assessed likelihood of the incident: Unlikely (1)

Comment to likelihood assessment:

[Ingen registreringer]

Assessment of risk for the consequence area: Helse

Assessed likelihood (common for incident): Unlikely (1)

Assessed consequence: Medium (2)

Comment to consequence assessment:

[Ingen registreringer]

Use of high temperature furnaces/Burn damage (incident)

Overall assessed likelihood of the incident: Less likely (2)

Comment to likelihood assessment:

[Ingen registreringer]

Assessment of risk for the consequence area: Helse

Assessed likelihood (common for incident): Less likely (2)

Assessed consequence: Medium (2)

Comment to consequence assessment:

[Ingen registreringer]

Use of compressed gases (He,Ar)/Uncontrolled expansion and depleiton of O2 (incident)

Overall assessed likelihood of the incident: Less likely (2)

Comment to likelihood assessment:

[Ingen registreringer]

Assessment of risk for the consequence area: Helse

Assessed likelihood (common for incident): Less likely (2)

Assessed consequence: Medium (2)

Comment to consequence assessment:

[Ingen registreringer]

Use of compressed gases (He,Ar)/Gas leakage (incident)

Overall assessed likelihood of the incident: Likely (3)

Comment to likelihood assessment:

[Ingen registreringer]

Assessment of risk for the consequence area: Helse

Assessed likelihood (common for incident): Likely (3)

Assessed consequence: Small (1)

Comment to consequence assessment:

[Ingen registreringer]

Use of aluminium, cobalt and nickel precursors (hazard)

Use of aluminium, cobalt and nickel precursors/Spills on skin (incident)

Overall assessed likelihood of the incident: Likely (3)

Comment to likelihood assessment:

[Ingen registreringer]

Assessment of risk for the consequence area: Helse

Assessed likelihood (common for incident): Likely (3)

Assessed consequence: Small (1)

Comment to consequence assessment:

[Ingen registreringer]

Use of flammable gases (CH4,H2) (hazard)

Use of flammable gases (CH4,H2)/Fire, explosion (incident)

Overall assessed likelihood of the incident: Unlikely (1)

Comment to likelihood assessment:

[Ingen registreringer]

Assessment of risk for the consequence area: Helse

Assessed likelihood (common for incident): Unlikely (1)

Assessed consequence: Medium (2)

Comment to consequence assessment:

[Ingen registreringer]

Use of flammable gases (CH4,H2)/Inhalation/Leakage (incident)

Overall assessed likelihood of the incident: Less likely (2)

Comment to likelihood assessment:

[Ingen registreringer]

Assessment of risk for the consequence area: Helse

Assessed likelihood (common for incident): Less likely (2)

Assessed consequence: Medium (2)

Comment to consequence assessment:

[Ingen registreringer]

Use of acetone for cleaning (hazard)

Use of acetone for cleaning/Spills on skin (incident)

Overall assessed likelihood of the incident: Likely (3)

Comment to likelihood assessment:

[Ingen registreringer]

Assessment of risk for the consequence area: Helse

Assessed likelihood (common for incident): Likely (3)

Assessed consequence: Small (1)

Comment to consequence assessment:

[Ingen registreringer]

Grinding and sieving of catalytic samples (hazard)

Grinding and sieving of catalytic samples/Inhaling of harmful particles (incident)

Overall assessed likelihood of the incident: Less likely (2)

Comment to likelihood assessment:

[Ingen registreringer]

Assessment of risk for the consequence area: Helse

Assessed likelihood (common for incident): Less likely (2)

Assessed consequence: Large (3)

Comment to consequence assessment:

[Ingen registreringer]

Appendix C

Table C.1: Catalyst composition data from XRF

Catalyst	**NiO** [%]	**MgO** [%]	**Al_2O_3** [%]	**Co_2O_3** [%]
NiCo-10	1.8	69.9	23.7	4.6
NiCo-20	4.3	59.8	25.6	10.2
NiCo-30	6.8	52.3	24.8	16.2
NiCo-40	9.8	40.0	27.0	23.2

Appendix D

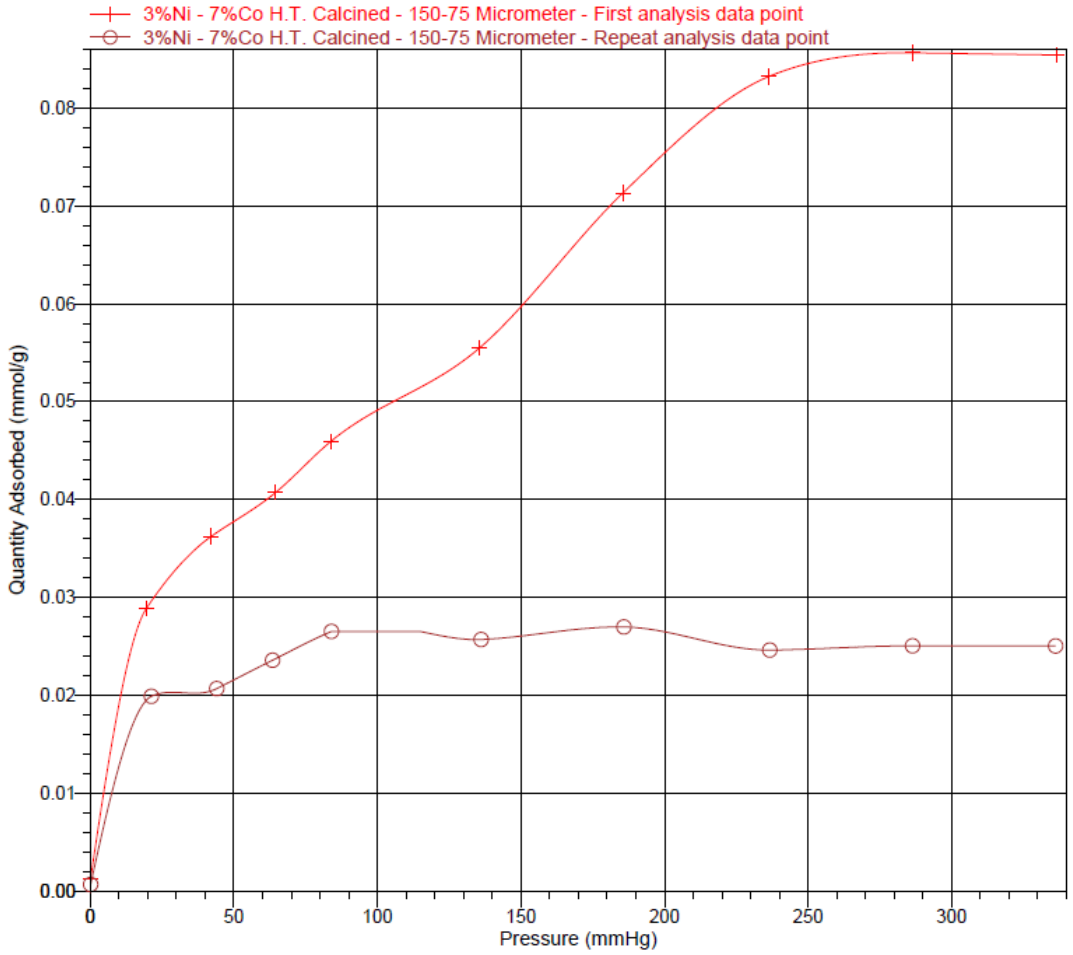

Figure D.1: Hydrogen chemisorption isotherm plot for NiCo-10

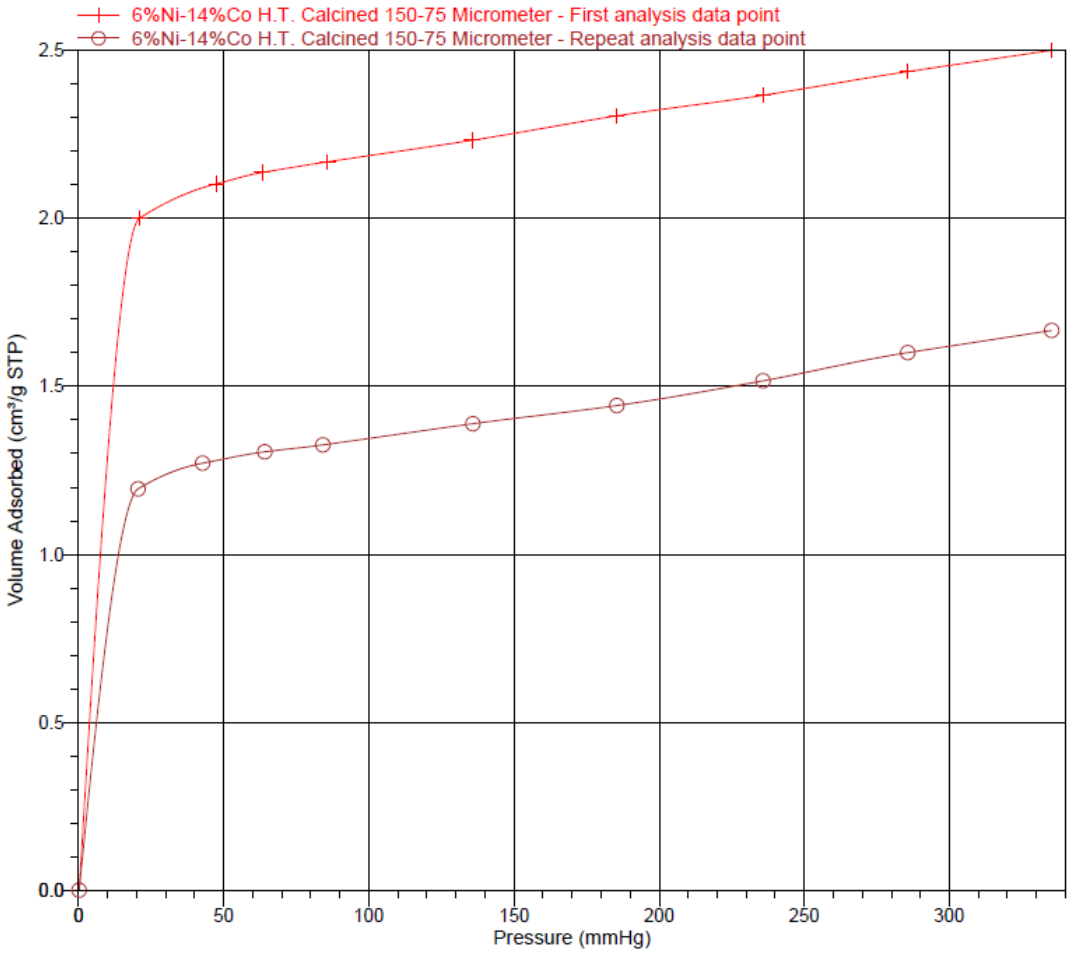

Figure D.2: Hydrogen chemisorption isotherm plot for NiCo-20

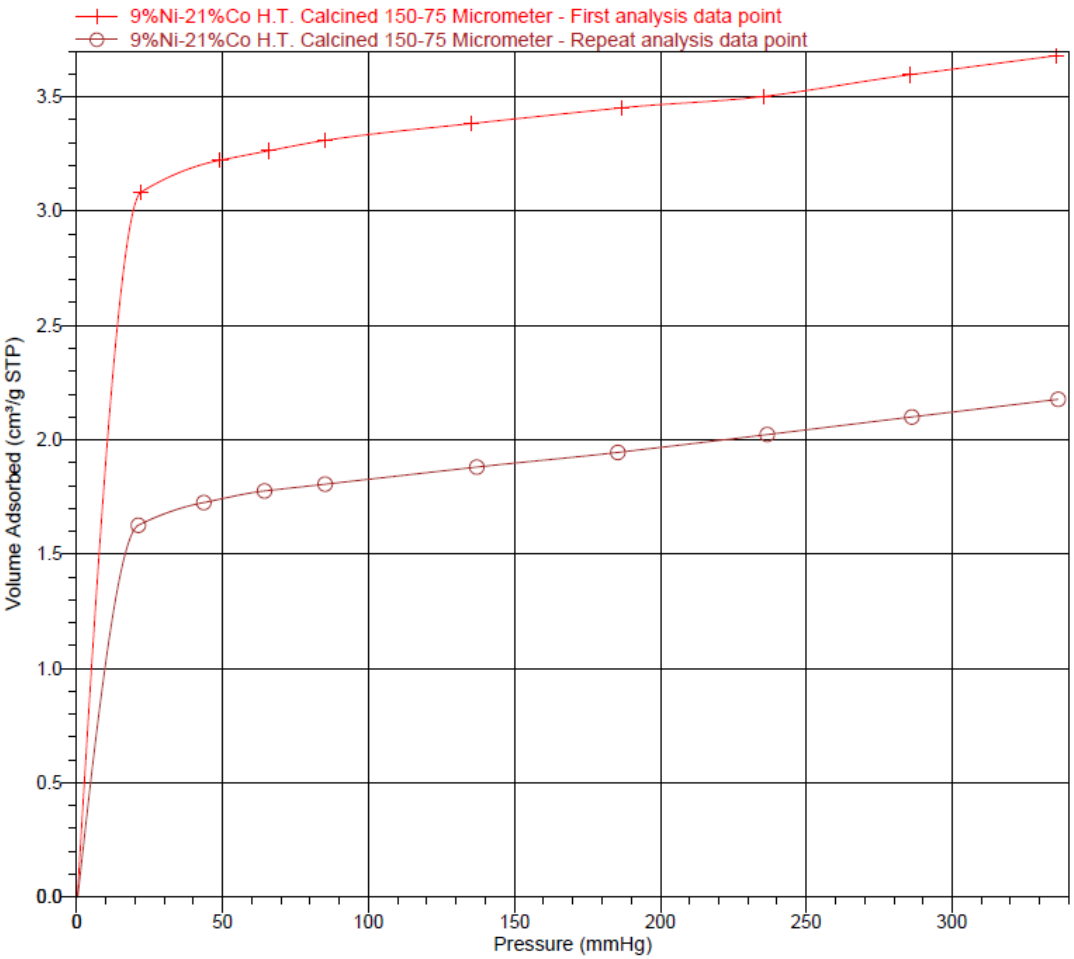

Figure D.3: Hydrogen chemisorption isotherm plot for NiCo-30

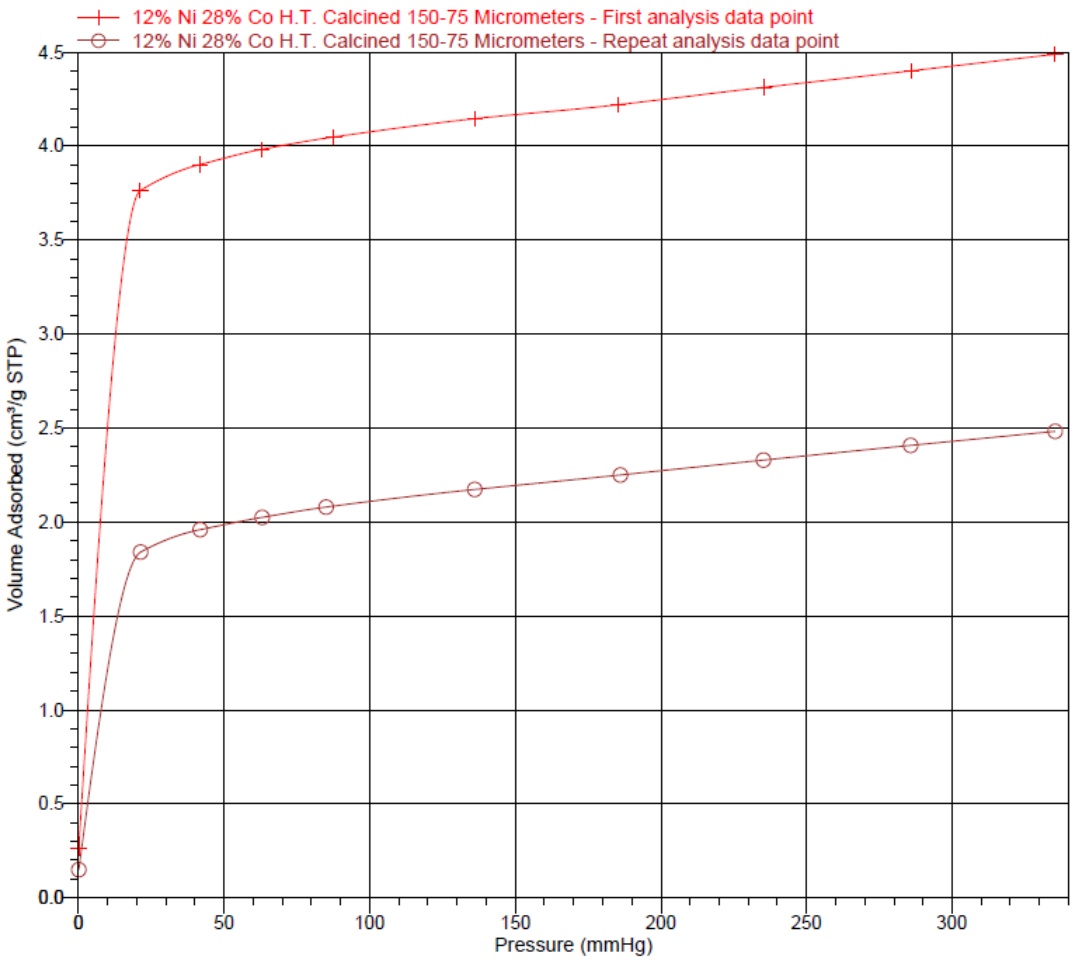

Figure D.4: Hydrogen chemisorption isotherm plot for NiCo-40

Appendix E

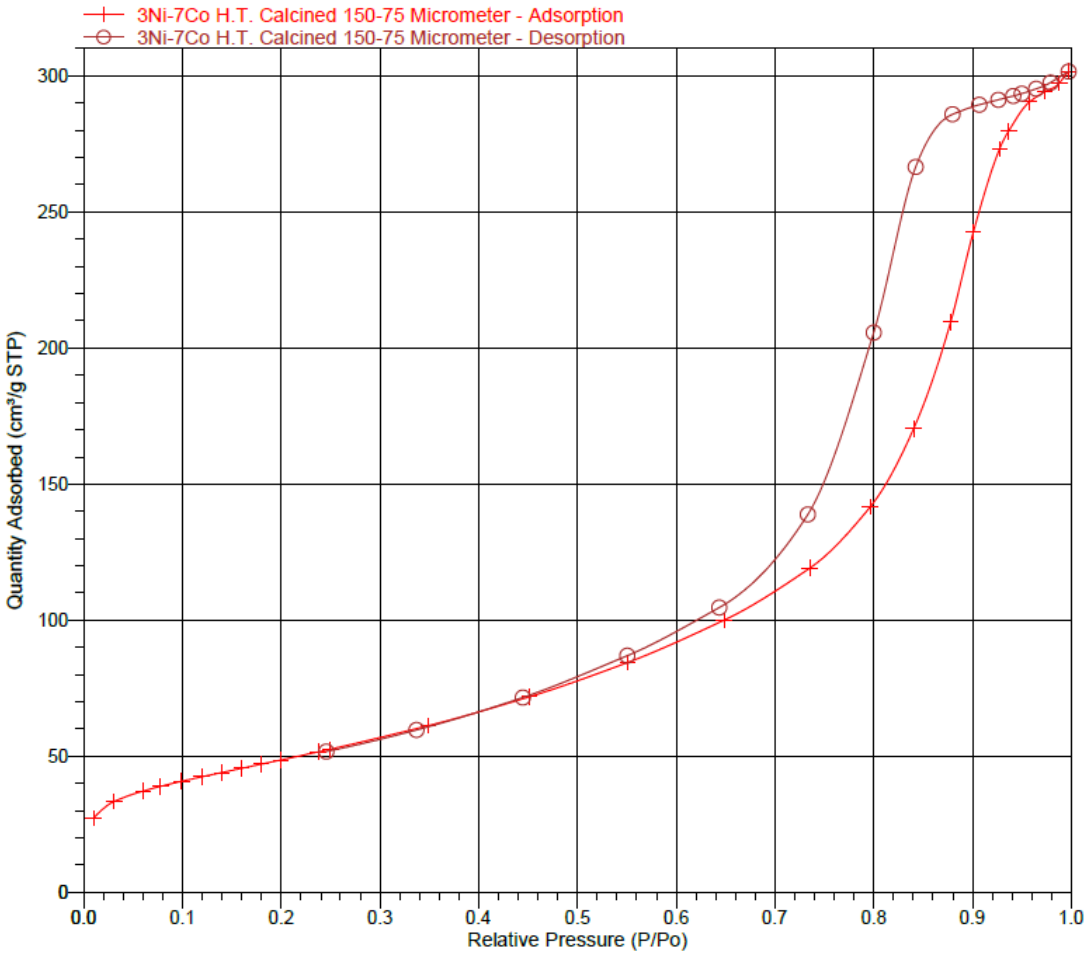

Figure E.1: Nitrogen adsorption linear isotherm plot for NiCo-10

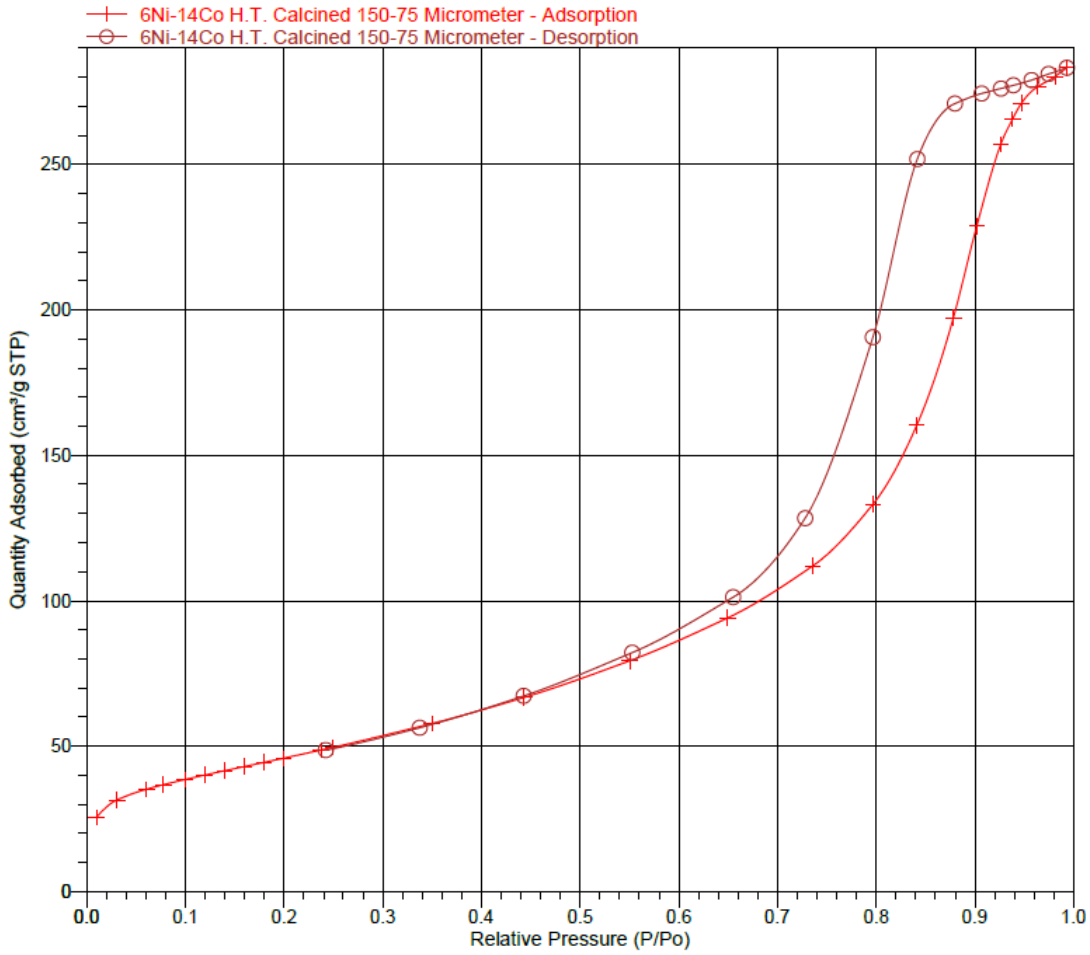

Figure E.2: Nitrogen adsorption linear isotherm plot for NiCo-20

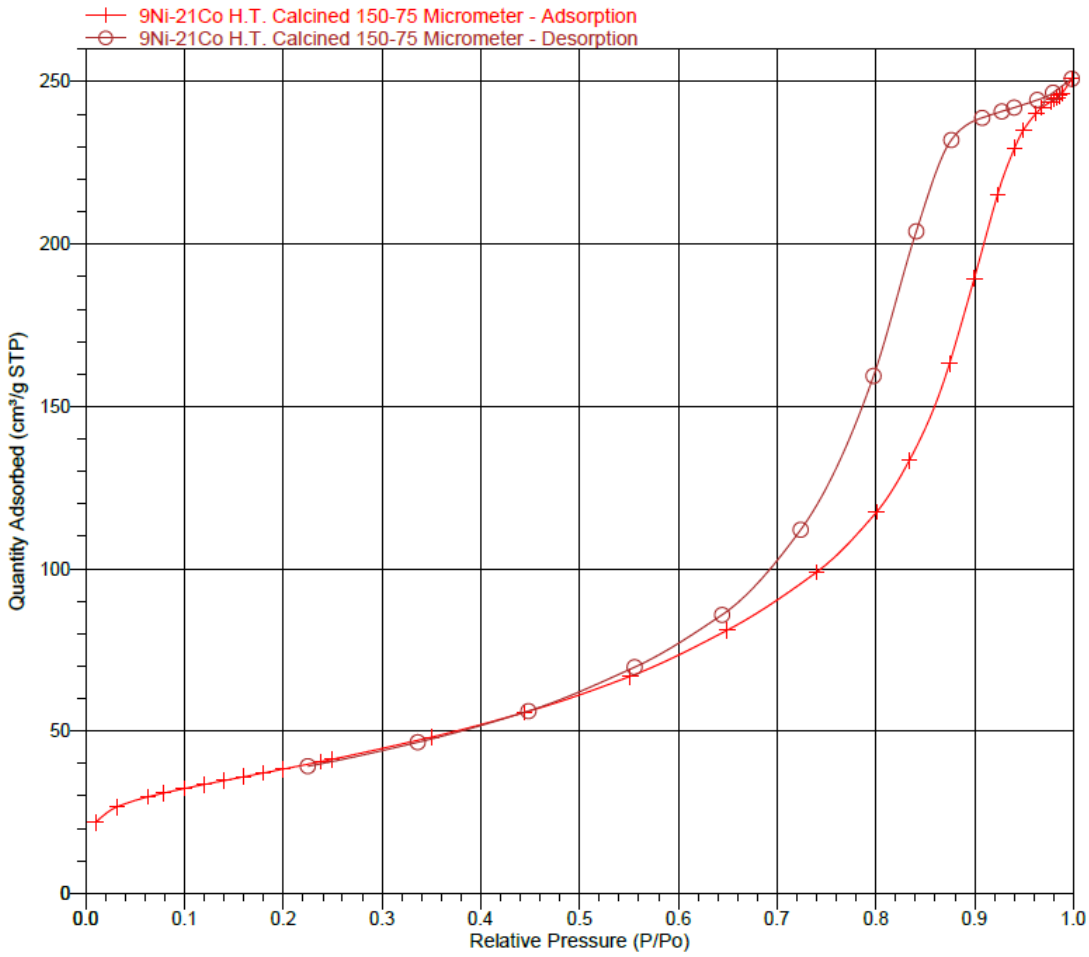

Figure E.3: Nitrogen adsorption linear isotherm plot for NiCo-30

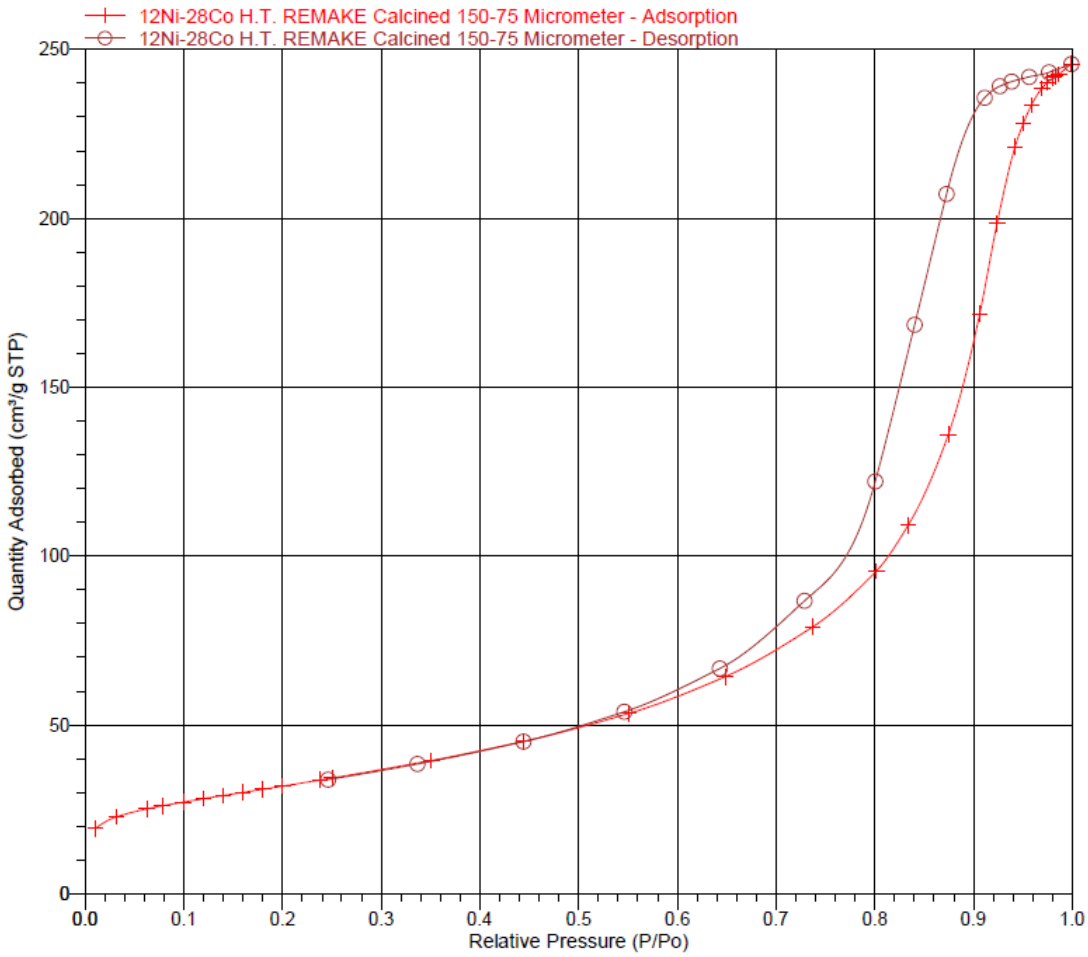

Figure E.4: Nitrogen adsorption linear isotherm plot for NiCo-40

Appendix F

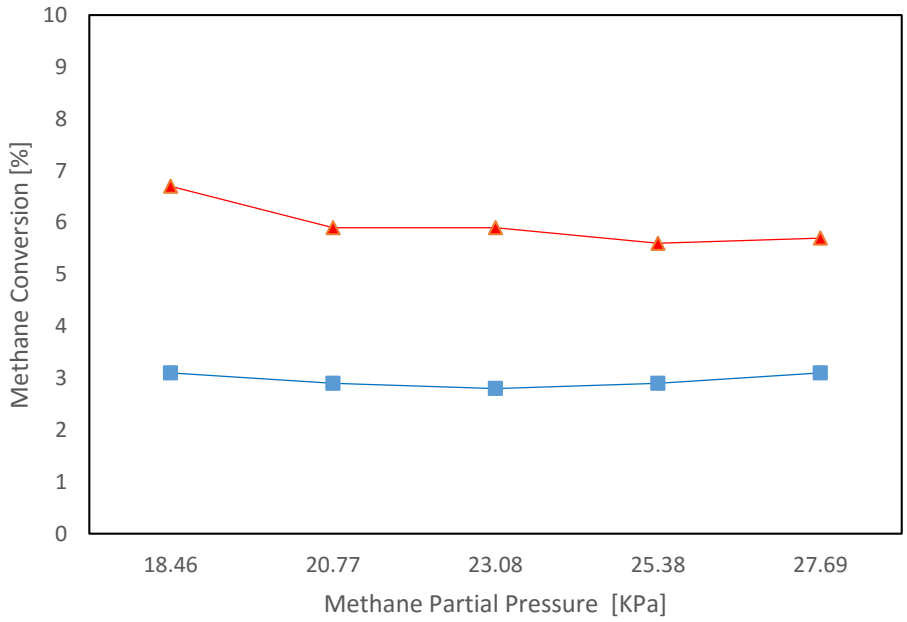

Figure F.1: Variation of methane conversion with methane partial pressure at 550 °C and 100 KPa, total flow is 412.5 ml/min and S:C ratio is 3.5:1. ■ NiCo-10, ▲ NiCo-40

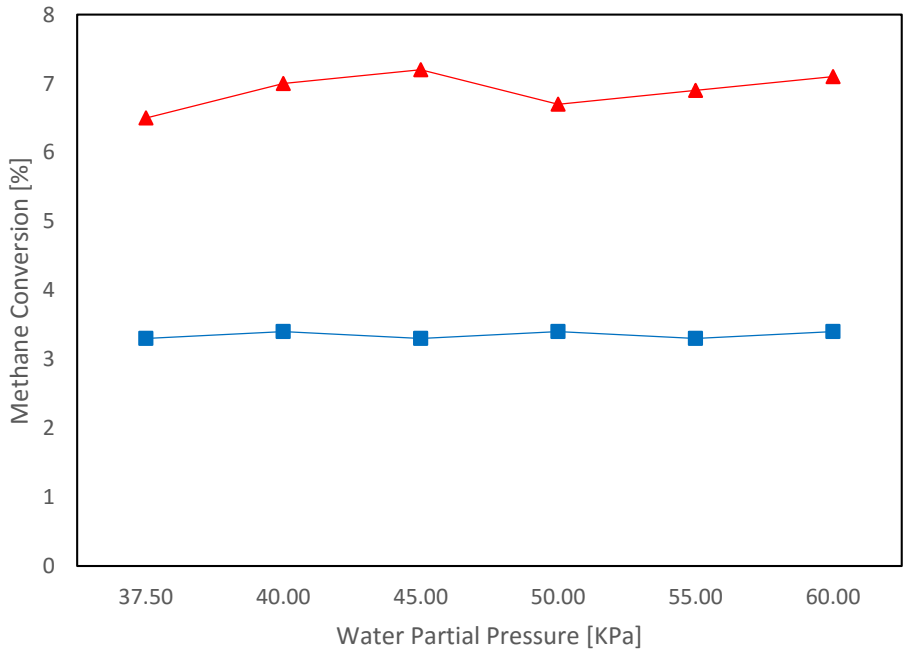

Figure F.2: Variation of methane conversion with water partial pressure at 550 °C and 100 KPa, total flow is 400 ml/min. ■ NiCo-10, ▲ NiCo-40

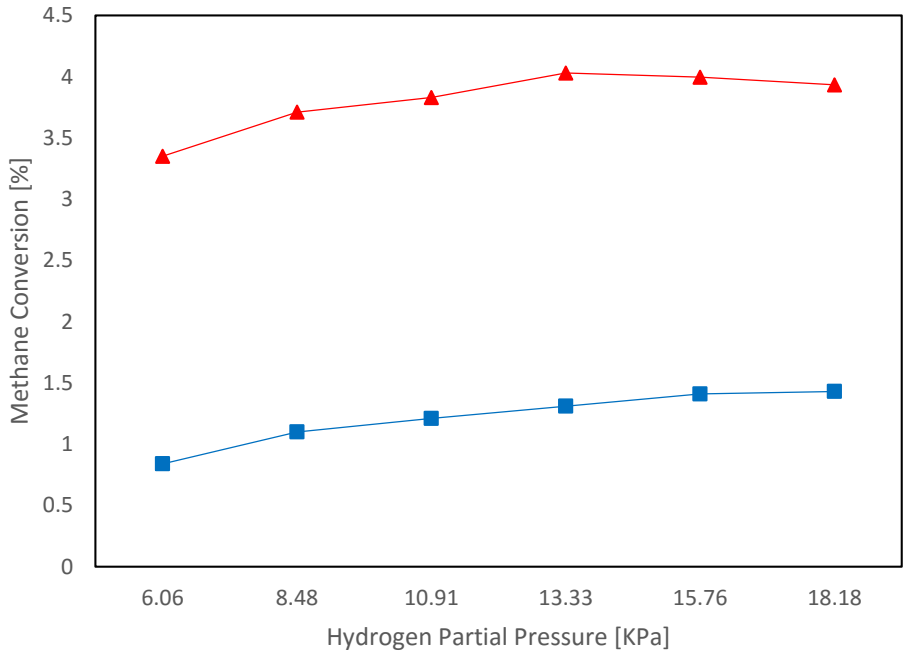

Figure F.3: Variation of methane conversion with hydrogen partial pressure at 550 °C and 100 KPa, total flow is 412.5 ml/min and S:C ratio is 3.5:1. ■ NiCo-10, ▲ NiCo-40